THE JOURNAL OF PHYSICAL CHEMISTRY A

Article

pubs.acs.org/JPCA

Secondary Organic Aerosol Formation from Low-NO_x Photooxidation of Dodecane: Evolution of Multigeneration Gas-Phase Chemistry and Aerosol Composition

Lindsay D. Yee,[†] Jill S. Craven,[‡] Christine L. Loza,[‡] Katherine A. Schilling,[‡] Nga Lee Ng,[§] Manjula R. Canagaratna,[∥] Paul J. Ziemann,[⊥] Richard C. Flagan,[†,‡] and John H. Seinfeld*[,†,‡]

[†]Division of Engineering and Applied Science, California Institute of Technology, Pasadena, California 91125, United States

[‡]Division of Chemistry and Chemical Engineering, California Institute of Technology, Pasadena, California 91125, United States

[§]School of Chemical and Biomolecular Engineering and School of Earth and Atmospheric Sciences, Georgia Institute of Technology, Atlanta, Georgia 30332, United States

[∥]Aerodyne Research, Inc., Billerica, Massachussets 01821, United States

[⊥]Air Pollution Research Center, Department of Environmental Sciences and Environmental Toxicology Graduate Program, University of California, Riverside, California 92521, United States

Supporting Information

ABSTRACT: The extended photooxidation of and secondary organic aerosol (SOA) formation from dodecane ($C_{12}H_{26}$) under low-NO_x conditions, such that RO_2 + HO_2 chemistry dominates the fate of the peroxy radicals, is studied in the Caltech Environmental Chamber based on simultaneous gas and particle-phase measurements. A mechanism simulation indicates that greater than 67% of the initial carbon ends up as fourth and higher generation products after 10 h of reaction, and simulated trends for seven species are supported by gas-phase measurements. A characteristic set of hydroperoxide gas-phase products are formed under these low-NO_x conditions. Production of semivolatile hydroperoxide species within three generations of chemistry is consistent with observed initial aerosol growth. Continued gas-phase oxidation of these semivolatile species produces multifunctional low volatility compounds. This study elucidates the complex evolution of the gas-phase photooxidation chemistry and subsequent SOA formation through a novel approach comparing molecular level information from a chemical ionization mass spectrometer (CIMS) and high m/z ion fragments from an Aerodyne high-resolution time-of-flight aerosol mass spectrometer (HR-ToF-AMS). Combination of these techniques reveals that particle-phase chemistry leading to peroxyhemiacetal formation is the likely mechanism by which these species are incorporated in the particle phase. The current findings are relevant toward understanding atmospheric SOA formation and aging from the "unresolved complex mixture," comprising, in part, long-chain alkanes.

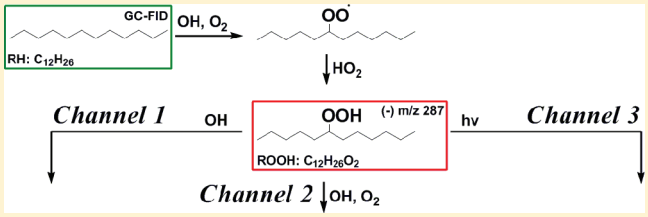

INTRODUCTION

Atmospheric chemical transformations occur through mechanisms involving free radical reactions, sunlight, and reactions in or on condensed media.[1] The formation of secondary organic aerosol (SOA) involves the multigeneration oxidation of a parent organic molecule leading to product molecules that partition between the gas and particle phases. As the parent organic is consumed, usually by reaction with the hydroxyl (OH) radical, subsequent products may also react with OH, giving rise to an evolving product distribution. As products become more functionalized with oxygen-containing moieties, their volatility decreases, and their propensity to partition into the particle phase increases.[2] In the gas-phase chemical cascade, both functionalization and fragmentation (C−C bond scission) reactions occur, and the interplay between these two general types of reactions, together with the progressive decrease in volatility accompanying the addition of oxygen atoms to the parent backbone, defines the SOA formation process for a particular parent organic.[3] As the SOA formation process evolves, a competition ensues between the rate of production of lower volatility species with increasing oxygen-to-carbon (O:C) atomic ratio and the increase in the SOA mass; as the mass of SOA increases, the partitioning of gas-phase products with somewhat higher volatility and somewhat lower O:C ratio is enhanced. The mass of SOA can, in some cases, reach a maximum and decrease as gas-phase fragmentation reactions convert lower volatility species into higher volatility species, leading to evaporation of the lower volatility particle-phase species in an attempt to maintain gas-particle equilibrium. In

Special Issue: A. R. Ravishankara Festschrift

Received: November 30, 2011
Revised: March 16, 2012
Published: March 16, 2012

short, the rate at which oxygens are added via successive gas-phase reactions, the relative importance of fragmentation versus functionalization reactions, and the specific decrease in volatility attending the formation of oxidized species govern the evolution of the SOA mass.

Long-chain alkanes represent an especially important class of organics with respect to SOA formation. The so-called unresolved complex mixture (UCM) is likely an important source of unaccounted for SOA formation in the atmosphere,[4] and alkanes are a major component of that mixture.[5,6] Low-volatility vapors from the UCM are a source of "untraditional" SOA, as they evaporate from primary organic aerosol emissions upon dilution and undergo subsequent oxidation to form SOA.[4] Quantifying the SOA formation from long-chain alkanes will undoubtedly aid in closing the gap between observed atmospheric organic aerosol and that predicted by atmospheric models based on traditional biogenic and anthropogenic SOA precursors. SOA formation from alkane photooxidation has received study.[7−12] Alkane−OH reaction kinetics[13,14] and gas-phase chemistry in the presence of NO_x exhibit a product distribution that can lead to highly oxidized products.[7,9,10] Studies of alkane oxidation under low-NO_x conditions have also been carried out.[15] Importantly, owing to the relatively long lifetimes against OH reaction at typical ambient OH concentrations (on the order of 12 h to several days) and to a relatively rich information base on the kinetics and mechanisms of alkane oxidation reactions, long-chain alkanes represent an especially important class of compounds with respect to SOA formation. Finally, it is crucial to develop detailed chemical databases on the explicit pathways of SOA formation for classes of parent organics, which can serve as benchmarks for evaluation of empirical/statistical models of SOA formation.

The present work represents the first report on a comprehensive series of laboratory chamber experiments on SOA formation from long-chain alkanes. We focus here on SOA formation from dodecane under low-NO_x conditions. The low-NO_x regime of atmospheric chemistry is particularly important in the regional to remote atmosphere and is especially relevant to the chemical aging that is intrinsic to SOA formation. The key to atmospheric photooxidation chemistry is the fate of the alkyl peroxy radical (RO_2) formed after OH attack and O_2 addition. RO_2 can react with HO_2, RO_2, or NO_x, the distribution of which is critical for understanding radical propagation and sinks, as well as the pathways that lead eventually to SOA.[16,17] In atmospheric regions of low NO_x levels, the RO_2 radical will react preferentially with HO_2 and RO_2. In such regions, HO_2 concentrations are on the order of 10^9 molecules cm^{-3},[18−20] and the RO_2−HO_2 reaction is competitive with the reaction of RO_2 with NO_x. Generally, under such atmospheric conditions, the RO_2−HO_2 reaction, which leads to hydroperoxides, dominates over RO_2 self-reaction. We present here the first experimental study of SOA formation from dodecane oxidation in the regime in which the fate of the dodecane peroxy radical is dominated by the RO_2 + HO_2 regime of alkyl peroxy radical chemistry. The particular focus of the present work is the multigeneration gas-phase chemistry of dodecane oxidation that leads to SOA formation. We employ chemical ionization mass spectrometry (CIMS) to track the evolution of the gas-phase oxidation products. We develop a gas-phase mechanism to describe the low-NO_x regime of chemistry. The mechanism is used to explicitly simulate four generations of gas-phase chemistry. By combining CIMS and high-resolution time-of-flight aerosol mass spectrometer (HR-ToF-AMS) measurements, we are able to simultaneously track several semivolatile oxidation products in the gas and particle phases. Together, these measurements provide evidence of particle-phase formation of peroxyhemiacetals (PHAs).

EXPERIMENTAL SECTION

Instrumentation. Experiments were conducted in the dual 28 m^3 Teflon reactors in the Caltech Environmental Chamber described elsewhere.[21,22] The reactors are flushed with clean, dry air for 24 h before a new experiment. A suite of online gas- and particle-phase instruments was used to monitor the development of the chemistry from dodecane photooxidation. The dodecane decay was monitored by taking hourly samples at 0.13 LPM of chamber air over 10 min (1.3 L total sample volume) onto a Tenax adsorbent. This was then loaded into the inlet of a gas chromatograph with flame ionization detection (GC/FID, Agilent 6890N), desorbed, and then injected onto an HP-5 column (15 m × 0.53 mm ID × 1.5 μm thickness, Hewlett-Packard). Desorption was at 270 °C for 15 min onto the column held at 30 °C. Next the oven was ramped from 30 to 280 °C at 10 °C/min and held at 280 °C for 5 min. The mass response of the detector was calibrated by spiking the Tenax cartridges with 0.5 μL of standard solution and analyzing them following the previously described method. Standard solutions of 25 mL volume each with concentrations ranging from 1 mM to 11 mM of dodecane in cyclohexane were prepared for these calibrations. The O_3 and NO_x were monitored using a standard UV absorption O_3 analyzer (Horiba, APOA 360) and a chemiluminescence NO_x analyzer (Horiba, APNA 360). During the injection period and before lights on, the temperature was around 293−294 K. After lights on, the temperature for all experiments ranged between 296 and 298 K, and relative humidity levels remained <5%.

The gas-phase chemistry was tracked using measurements from a CIMS, consisting of a modified Varian 1200 quadrupole mass spectrometer to accommodate a custom ionization region. The general operation and details of the instrument have been discussed previously.[23−25] In negative mode operation, the use of CF_3OOCF_3 reagent gas makes the instrument ideal for measuring hydroperoxide containing compounds and acidic species, as described in studies of CF_3OOCF_3 chemistry.[26] For a more strongly acidic species [H·X], the transfer product is formed during ionization $[H{\cdot}X{\cdot}F]^-$, resulting in a nominal mass-to-charge ratio, m/z, of $[M+19]^-$, where M is the molecular weight of the analyte. For less acidic species and hydroperoxides [R], the cluster product forms $[R{\cdot}CF_3O]^-$, or m/z = $[M+85]^-$. Carboxylic acids such as acetic and formic acids tend to have equal contributions to the transfer and cluster product, in which case the overall signal of a compound is considered as the sum of the two product channels. In positive mode operation, an analyte R can undergo proton transfer reaction generating an ion of the form $[R{\cdot}H]^+$ and/or react with n positively charged water clusters to form a cluster in the form of $[(H_2O)_n{\cdot}R{\cdot}H]^+$. Hydroperoxide species tend to undergo dehydration after protonation, and are thus monitored at nominal m/z = $[M-17]^+$.[27] Unfortunately, due to mass tuning shifts midproject, the positive mode m/z's reported do not reflect the expected m/z from the clustering theory, but use of this mode of the CIMS was essential for tracking less polar compounds such as the carbonyl and, in some instances, where product m/z's were out of range for the mass scan in negative

Table 1. Dodecane Low-NO_x Experiments

expt date	hrs of photooxidation	initial HC (ppb)	$[NO]_0$ (ppb)	$[NO_x]_0$ (ppb)	$[O_3]_0$ (ppb)	initial seed vol. ($\mu m^3 cm^{-3}$)	ΔHC (ppb)	peak organic[a] ($\mu g\ cm^{-3}$)
1/16/2011	18	34.2 ± 1.6	<LDL	<LDL	2.7	9.1 ± 0.3	32.0 ± 2.1	54.6
3/13/2011	36	34.9 ± 1.6	<LDL	<LDL	2.6	11.4 ± 1.5	33.6 ± 2.1	62.8
3/16/2011	18	33.0 ± 1.6	<LDL	<LDL	3.3	12.0 ± 1.2	32.3 ± 2.1	51.3

[a]Not corrected for particle wall loss.

mode operation. The positve mode m/z's are reported as monitored during the experiment, but suggested assignments were made using a back calibration of the shift of m/z, generally upward by five atomic mass units (amu) in the m/z range of interest from 200 to 220. While the CIMS is capable of measuring a diverse array of chemical species, specificity is challenged when isomers or different compounds with the same nominal MW contribute to the same m/z signal, which has unit mass resolution. In this study, many isomers are formed because there are many possible locations of hydroxyl radical attack on the starting chain. The CIMS signal at one m/z represents the summed contribution of all the isomers. Isomeric compounds in this study were mostly problematic for distinguishing the acids, in that one cannot fully distinguish the difference between a C_n peracid, C_n hydroxycarboxylic acid, and a C_{n+1} hydroperoxide, as discussed in the results section on acid formation.

Particle size distribution and number concentration measurements are made with a cylindrical differential mobility analyzer (DMA; TSI Model 3081) coupled to a condensation particle counter (TSI Model 3010). A logarithmic scan from a mobility diameter of 10 nm to 1 μm is completed every 90 s. Sheath and excess flows of 2.5 LPM were used, with a 5:1 flow rate ratio of sheath-to-aerosol (i.e., a resolving power of 5). An Aerodyne HR-ToF-AMS,[28−30] hereafter referred to as the AMS, continuously measured submicrometer nonrefractory aerosol composition at 1 min resolution switching between the higher resolution, lower sensitivity W mode and the lower resolution, higher sensitivity V mode. A detailed discussion of the AMS method for the automated m/z calibration, mass accuracy, mass resolution of V and W modes, the high-resolution ion fitting algorithm, and ion signal integrations at the same integer mass is presented in previous work.[29] The AMS ions (organic) are reported with a relative ionization efficiency of 1.4.[30]

Experimental Protocols. To maximize total OH exposure, a set of experiments was designed following phased instrument sampling protocols similar to those used in the work of Loza et al.[31] to capture 36 h of total photooxidation while preserving reactor volume. In this study, the 36 h time series is achieved by combining data from an 18 h experiment during which all instruments are online and a 36 h experiment during which all instruments but the AMS are offline during the first 20 h of oxidation. Relative humidity and temperature were monitored for the full 36 h. Thus, the concatenated time series for many instruments (i.e., the CIMS, DMA, NO_x, and O_3 analyzers) is that of the 18 h experiment and the last 16 h of the 36 h experiment. A list of the experiments used for this study are in Table 1. The March experiments used another DMA with a lower total effective flow rate. General consistency between the AMS and CIMS measurements across the two 18 h experiments is observed (see Supporting Information, Figure S1). In the 18 h January experiment, CIMS traces for negative mode ions at $m/z > 300$ were included; the mass scan was reduced to $m/z \leq 300$ in the March experiments. The January experiment also provided evidence for supporting alternate positive mode m/z's used for monitoring select hydroperoxide species in the March experiments, which would otherwise be best monitored by the negative mode in the m/z range >300 (see Supporting Information, Figure S2).

Injection protocols were the same for all experiments. Two-hundred eighty microliters of a 50% by weight solution of hydrogen peroxide in water was measured using a glass syringe and injected into a glass trap. The trap was submerged in a warm water bath (~35−38 °C) while 5 LPM of the purified injection air flowed through the trap and into the chamber evaporating the hydrogen peroxide over approximately 90 min. This results in an approximate starting hydrogen peroxide concentration of 4 ppm. Next a 0.015 M aqueous ammonium sulfate solution was atomized into the chambers providing ~11 $\mu m^3/cm^3$ volume concentration of seed prior to lights on, as measured by the chamber DMA. Finally, 9 μL of dodecane (Sigma-Aldrich, 98% purity) was injected into a glass bulb and connected within six inches to a reactor injection port via 1/4″ o.d. polytetrafluoroethylene (PTFE) tubing. This led to a 10 inch line of 1/4″ o.d. PTFE internal to the reactor from the injection port to ensure injection would not be directly to the reactor wall. Using a heat gun with gentle heat, the dodecane evaporated into a flow of 5 LPM of purified injection air going into the chamber. This injection method was performed as close to the chamber as possible to prevent losses of the parent hydrocarbon during line transfer. The resulting dodecane concentration in the chamber was about 34 ppb. Each experiment's starting concentration is listed in Table 1. After loading the reactors, an hour period elapsed to allow for mixing. Then, the blacklights were turned on initiating generation of the OH radical from H_2O_2 photolysis.

Experimental Controls. A thorough discussion on characterizations of the particle-phase wall loss for longer experiments in the Caltech Environmental Chamber appears elsewhere.[31] For this study, we estimate that by 18 and 36 h of oxidation, approximately 15% and finally 28% of the particle volume has been lost to the walls when comparing DMA suspended volume and wall loss corrected particle volume. A diagnostic dark vapor-phase wall-loss experiment was performed by injecting 60 ppb 2-dodecanone into the chamber and monitoring its decay in the dark over 22 h. Although there was an observed loss of 14% CIMS dodecanone signal over 22 h from its initial signal after injection, one cannot eliminate the possibility of immediate wall-loss or transfer loss during the injection and mixing period (~75 min total). Because handling of the standard proved difficult for establishing a confident calibration curve for the CIMS, this could not be verified. No appreciable formation of > C_3 acids and hydroperoxide species above the background noise from the CIMS measurements was observed, and no aerosol volume above the limit of detection (~0.6 $\mu m^3\ cm^{-3}$) was produced by 22 h as measured by the DMA. Further investigation would be necessary for the goal of mass closure. In order to verify the fragmentation pattern of

dx.doi.org/10.1021/jp211531h | J. Phys. Chem. A 2012, 116, 6211−6230

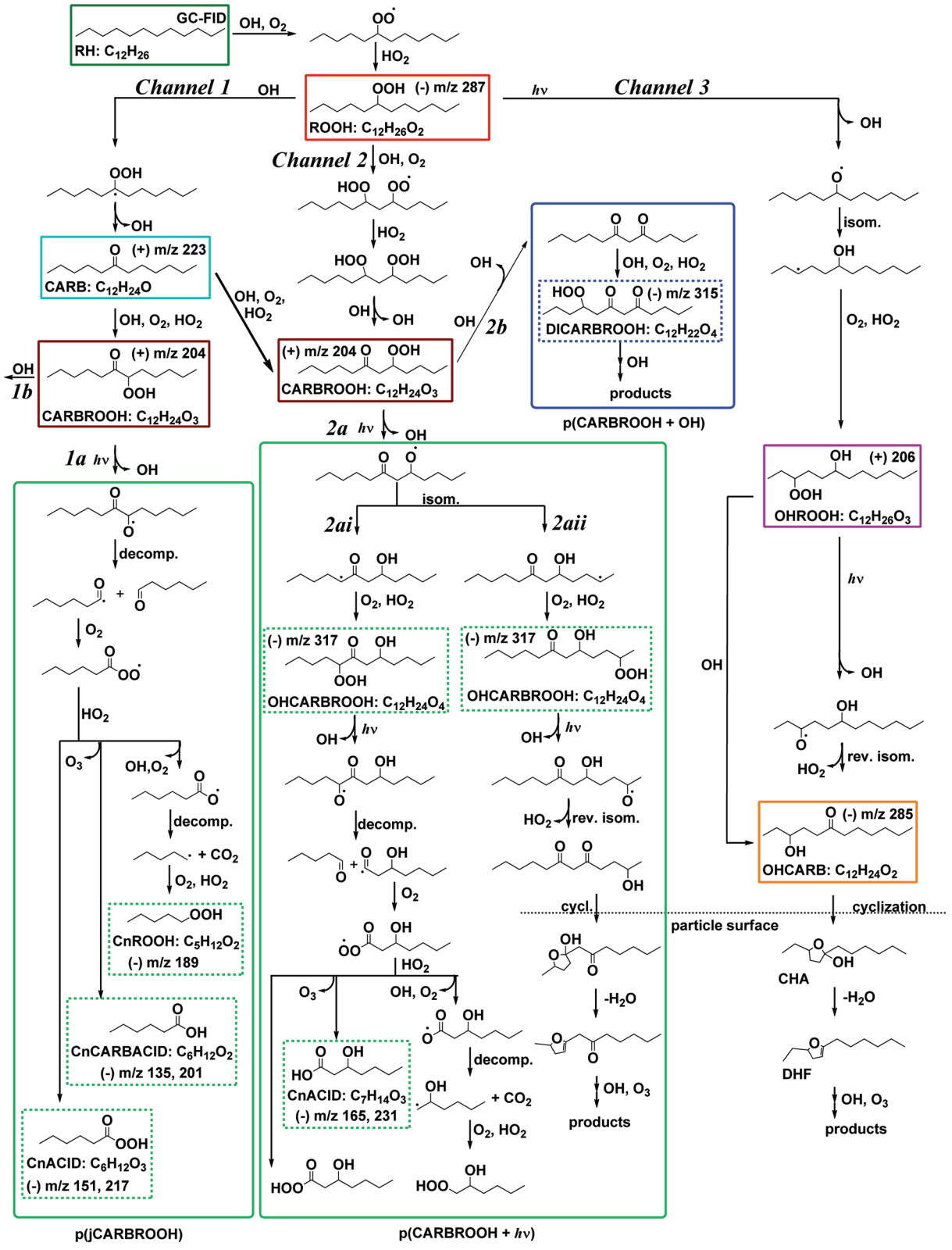

Figure 1. Dodecane low-NO_x mechanism. This scheme explicitly shows OH attack at the C_6 position; however, abstraction of other hydrogens on secondary carbons can also occur. Reaction of dodecane with OH forms a hydroperoxide (ROOH). The hydroperoxide undergoes successive reactions to generate the carbonyl hydroperoxide (CARBROOH, Channel 1 and Chanel 2) or photolyzes to form the hydroxy hydroperoxide (OHROOH, Channel 3). The solid colored boxes indicate compounds or reaction pathways photochemically simulated. CIMS monitored species have m/z noted. Dashed colored boxes indicate compounds monitored by CIMS, but not explicitly simulated in the photochemical mechanism. The gray dashed line denotes a gas−particle interface where 1,4-hydroxycarbonyl (OHCARB)-like compounds reactively uptake onto the particle and cyclize to form a cyclic hemiacetal (CHA).

dx.doi.org/10.1021/jp211531h | J. Phys. Chem. A 2012, 116, 6211−6230

Table 2. Reactions Included in the Gas-Phase Photochemical Model

rxn #	reaction	k	ref.
1	$H_2O_2 + h\nu \rightarrow 2OH$	$j_{H_2O_2} = 2.87 \times 10^{-6}\ s^{-1}$	JPL[37] + chamber irradiance data
2	$H_2O_2 + OH \rightarrow HO_2 + H_2O$	$k_1 = 1.8 \times 10^{-12}\ cm^3\ molecule^{-1}\ s^{-1}$	JPL[37]
3	$RH + OH \rightarrow RO_2 + H_2O$	$k_2 = k_{OH} = 13.2 \times 10^{-12}\ cm^3\ molecule^{-1}\ s^{-1}$	Atkinson, 1997[14]
4	$RO_2 + RO_2 + M \rightarrow pRO_2RO_2 + M$	$k_3 = 5 \times 10^{-15}\ cm^3\ molec^{-1}\ s^{-1}$	Atkinson, 1997[14]
5	$RO_2 + HO_2 \rightarrow ROOH + O_2$	$k_4 = 2.16 \times 10^{-11}\ cm^3\ molecule^{-1}\ s^{-1}$	MCM 3.2
6	$HO_2 + HO_2 \rightarrow H_2O_2 + O_2$	$k_5 = 1.5 \times 10^{-12}\ cm^3\ molec^{-1}\ s^{-1}$	JPL[37]
7	$OH + HO_2 \rightarrow H_2O + O_2$	$k_6 = 1.1 \times 10^{-10}\ cm^3\ molecule^{-1}\ s^{-1}$	JPL[37]
8	$OH + OH \rightarrow H_2O_2$	$k_7 = 6.28 \times 10^{-12}\ cm^3\ molec^{-1}\ s^{-1}$	JPL[37]
9	$ROOH + OH \rightarrow CARB$	$k_8 = 7.4 \times 10^{-12}\ cm^3\ molecule^{-1}\ s^{-1}$	JPL[37]
10	$ROOH + h\nu \rightarrow RO + OH$	$j_{ROOH} = 2.30 \times 10^{-6}\ s^{-1}$	MCM 3.2 + chamber irradiance data
11	$RO + O_2 \rightarrow OHRO_2$	$k_9 = 2.59 \times 10^{-6}\ cm^3\ molecule^{-1}\ s^{-1}$	MCM 3.2
12	$OHRO_2 + HO_2 \rightarrow OHROOH + O_2$	$k_{10} = k_4$	MCM 3.2
13	$CARB + OH \rightarrow CARBRO_2 + H_2O$	$k_{11} = 1.49 \times 10^{-11}\ cm^3\ molecule^{-1}\ s^{-1}$	MCM 3.2
14	$CARBRO_2 + HO_2 \rightarrow CARBROOH$	$k_{12} = k_4$	MCM 3.2
15	$CARB + h\nu \rightarrow pjCARB$	$j_{CARB} = 3.32 \times 10^{-7}\ s^{-1}$	MCM 3.2 + chamber irradiance data
16	$CARBROOH + OH \rightarrow p(CARBROOH + OH)$	$k_{13} = 9.10 \times 10^{-11}\ cm^3\ molecule^{-1}\ s^{-1}$	MCM 3.2
17	$CARBROOH + h\nu \rightarrow p(jCARBROOH)$, aka $p(CARBROOH + h\nu)$	j_{ROOH}	MCM 3.2 + chamber irradiance data
18	$OHROOH + OH \rightarrow OHCARB$	$k_{14} = 4.97 \times 10^{-11}\ cm^3\ molecule^{-1}\ s^{-1}$	MCM 3.2
19	$OHROOH + h\nu \rightarrow pjOHROOH$	j_{ROOH}	MCM 3.2 + chamber irradiance data
20	$pjOHROOH \rightarrow OHCARB + HO_2$	$k_{15} = 2.83 \times 10^{7}\ cm^3\ molecule^{-1}\ s^{-1}$	MCM 3.2
21	$RO_2 + NO \rightarrow 0.56\ RO + 0.44\ pRONO_2$	$k_{16} = 9.04 \times 10^{-12}\ cm^3\ molecule^{-1}\ s^{-1}$	MCM 3.2
22	$OHRO_2 + NO \rightarrow 0.176\ OHRO + 0.824\ pOHRONO_2$	$k_{17} = k_{16}$	MCM 3.2
23	$CARBRO_2 + NO \rightarrow CARBRO$	$k_{18} = k_{16}$	MCM 3.2
24	$OHRO_2 + RO_2 \rightarrow pOHRO_2RO_2$	$k_{19} = k_3$	MCM 3.2
25	$CARBRO_2 + RO_2 \rightarrow pCARBRO_2RO_2$	$k_{20} = k_3$	MCM 3.2
26	$RO_2 + NO_2 \rightarrow pRO_2NO_2$	$k_{21} = 9.0 \times 10^{-12}\ cm^3\ molecule^{-1}\ s^{-1}$	JPL[37]
27	$OHRO_2 + NO_2 \rightarrow pOHRO_2NO_2$	$k_{22} = k_{21}$	JPL[37]
28	$CARBRO_2 + NO_2 \rightarrow pCARBRO_2NO_2$	$k_{23} = k_{21}$	JPL[37]

hydroperoxide species in the AMS spectrum, a seeded photooxidation experiment was run with a target injection of 300 ppb octadecane ($C_{18}H_{38}$) using the experimental protocols discussed earlier. The first generation hydroperoxide ($C_{18}H_{38}O_2$) immediately partitions to the particle-phase, and a distinct AMS ion at nominal m/z = 253 ($C_{18}H_{37}^+$) appeared after lights on, suggesting that hydroperoxide species fragment to form ions of the form $[M\text{-}33]^+$, where M is the molecular weight of the hydroperoxide species.

DODECANE LOW-NO_X GAS-PHASE MECHANISM

The OH-initiated photoxidation of *n*-alkanes has been studied previously, providing a framework of well-known chemical reactions under varying NO_x conditions[14,15] that can be extended to the case of dodecane. Such reactions are also included in the Master Chemical Mechanism 3.2 (MCM 3.2) via Web site: http://mcm.leeds.ac.uk/MCM.[32,33] The reactions proposed in such previous studies in conjunction with gas-phase measurements from this study afforded the development of a mechanism for the photoxidation of dodecane under low-NO_x conditions where $RO_2 + HO_2$ chemistry dominates (see Figure 1). Reaction pathways past the carbonyl hydroperoxide (CARBROOH) along Channel 1a and Channel 2b are not included in the MCM 3.2 for dodecane. For clarity, colored boxed molecules with simple labels are those that were explicitly simulated in the photochemical mechanism and are represented in the reactions of Table 2, consistent with the color scheme comparing CIMS measurements and simulated output in Figure 2 (RH, ROOH, CARB, CARBROOH, OHROOH, and OHCARB). In some cases, a group of products was not modeled explicitly, so a reaction pathway is boxed and labeled (p(jCARBROOH), p(CARBROOH + hν), and p(CARBROOH + OH)). Boxed molecules with a dashed border indicate those that have been monitored by the CIMS including the m/z that was monitored, but they were not explicitly modeled in the photochemical mechanism (CnROOH, CnCARBACID, CnACID, OHCARBROOH, and DICARBROOH). Reaction channels are noted with alphanumeric labels, and the labels for molecules or product channels of interest are referred to throughout the text. OH attack is explicitly shown at the C_6 carbon, although it is expected that any of the hydrogens on secondary carbons will be similarly vulnerable to abstraction by the OH radical. Using estimated structure activity relationship reaction rate constants,[34] OH abstraction of the hydrogens on the primary carbons would only represent two percent of the overall reaction rate of dodecane with OH. Five generations of chemistry are represented in the reaction pathways of Figure 1, with a generation defined as the OH-initiated or photolysis reaction of a stable (nonradical) compound. The mechanism provides an overview of the types of products generated from the alkyl peroxy radical RO_2 exclusively reacting with HO_2 to generate hydroperoxides, which then react with OH or undergo photolysis. While a wide variety of compounds are included in the mechanism shown in Figure 1, this mechanism is by no means exhaustive of all possible compounds formed in terms of functional group placement and molecular structure.

Low-NO_x Conditions. Under conditions in which $[HO_2] \gg [RO_2]$, and in which NO_x levels are very low, RO_2 can be expected to react exclusively with HO_2. For the experimental conditions, the HO_2 is calculated by a photochemical model. The HO_2 concentration ($\sim 1 \times 10^{10}$ molecules cm^{-3}) exceeds

dx.doi.org/10.1021/jp211531h | J. Phys. Chem. A 2012, 116, 6211−6230

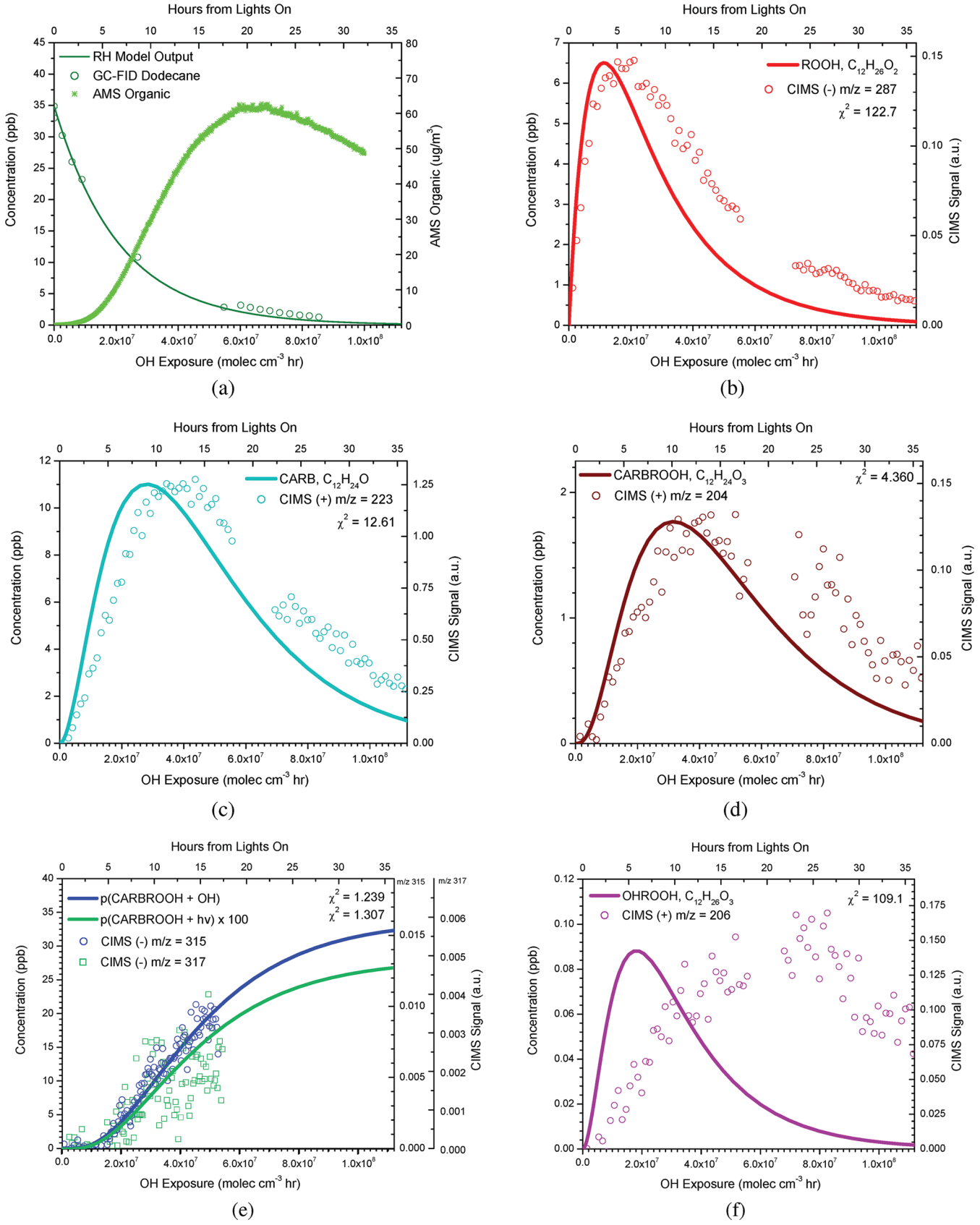

Figure 2. continued

dx.doi.org/10.1021/jp211531h | J. Phys. Chem. A 2012, 116, 6211−6230

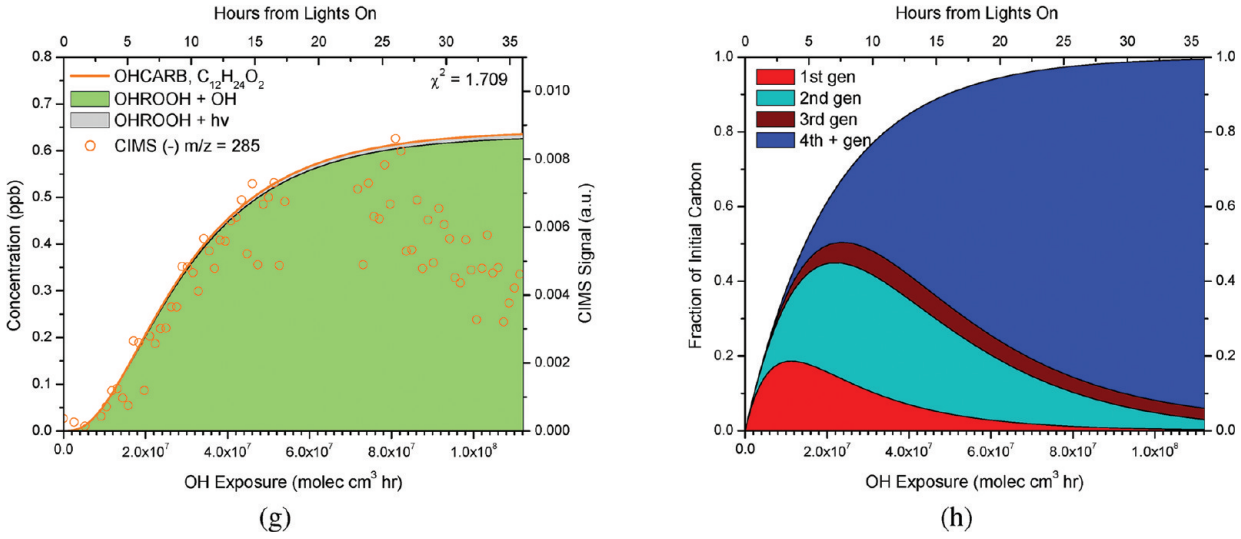

Figure 2. Simulated (curves) and observed (open circles) time evolutions of various gas-phase species from OH-initiated photoxidation of dodecane. Colors used match species outlined in the gas-phase mechanism. (a) Decay of dodecane parent hydrocarbon with suspended organic growth. (b) First-generation formation of the hydroperoxide (ROOH) monitored at (−) m/z 287. (c) Second-generation formation of the ketone (CARB) monitored at (+) m/z 223. (d) Third-generation formation of the carbonyl hydroperoxide (CARBROOH) monitored at (+) m/z 204. (e) Simulated output of remaining carbon from further oxidation of the carbonyl hydroperoxide p(CARBROOH + OH) as (−) m/z 315 or photolysis p(CARBROOH + hν) as (−) m/z 317. (f) Photolysis of the hydroperoxide (ROOH) leads to formation of a hydroxy hydroperoxide (OHROOH) monitored at (+) m/z 206. (g) Formation of the hydroxycarbonyl (OHCARB) from two sources: (1) photolysis of the hydroxy hydroperoxide (OHROOH + hν) and (2) OH reaction with the hydroxy hydroperoxide (OHROOH + OH). (h) Simulated fraction of initial carbon in the gas-phase by generation over the course of the experiment.

that of RO_2 (~1 × 10^8 molecules cm^{-3}) by 2 orders of magnitude. The dominant route of RO_2 chemistry is reaction with HO_2 to form hydroperoxide compounds. It is important to note that what determines low-NO_x or high-NO_x conditions is not merely dependent on the HO_2 concentration iteslf; rather, the conditions are defined by the dynamics of NO and RO_2 and the various reaction rate constants. For example, the reaction rate constants for CH_3O_2 with HO_2, CH_3O_2, NO, and NO_2 at 298 K are 5.2 × 10^{-12} cm^3 $molecule^{-1}$ s^{-1}, 3.7 × 10^{-13} cm^3 $molecule^{-1}$ s^{-1}, 6.5−7.8 × 10^{-12} cm^3 $molecule^{-1}$ s^{-1}, and 3.9 × 10^{-12} cm^3 $molecule^{-1}$ s^{-1}, respectively.[14] On the basis of these rate constants, CH_3O_2 lifetime against reaction with these species increases in the order of NO, HO_2, NO_2, and CH_3O_2. However, sufficient concentrations of HO_2 and/or CH_3O_2 as compared with NO would shift the conditions to an effectively low-NO_x regime of chemistry, in which the relative concentrations of HO_2 and CH_3O_2 would then determine whether the low-NO_x regime is dominated by CH_3O_2 + HO_2 or shared with CH_3O_2 + CH_3O_2.

Without any addition of NO_x, a small amount of NO_x, presumably from residual nitrogen-containing acids (e.g., HONO or HNO_3) on the chamber walls, is generated upon irradiation. This phenomenon of "NO_x offgasing"[35] is a common observation among environmental chambers.[35,36] In the chamber experiments to be described, the NO concentration is below the limit of detection (~ 5 ppb), and the NO_2 generated is <5 ppb. While the total generated NO_x is primarily in the form of NO_2, NO_2 cannot be calibrated directly with this technique, and there are fewer calibration points at this lower range leading to some uncertainty in the measurement. Low-NO_x conditions in the chamber are further verified by CIMS measurements of HO_2NO_2 pernitric acid (PNA), the formation of which is highly sensitive to the HO_2:NO_2 ratio. Using the CIMS sensitivity to PNA,[24] the PNA concentration generated upon lights on is <350 pptv. As discussed in the work of Paulot et al.,[24] it is likely that the sensitivity to PNA is overestimated due to ligand exchange of H_2O_2 with the reagent ion. Using the expected HO_2 concentration generated upon irradiation, and the equilibrium constant for HO_2 + NO_2 ⇌ HO_2NO_2, 1.6 × 10^{-11} cm^3 $molec^{-1}$,[37] the predicted NO_2 residual concentration is <1.2 ppb.

To explore possible effects of residual NO_x, the chemistry was simulated with initial concentrations of NO at 0.1 ppb, 2 ppb, and constant NO at 0.1 ppb, using all reactions in Table 2. Under these varying NO_x conditions, we estimate that <1%, < 10%, and <19%, respectively, of the dodecane reacts via RO_2 + NO_x reactions. Relative lifetimes of RO_2 against reaction with RO_2, HO_2, NO, and NO_2 for these varying NO_x conditions are provided in the Supporting Information, Table S1. The two species, the 1,4-hydroxycarbonyl (OHCARB, Figure 1) and the hydroxy hydroperoxide (OHROOH, Figure 1) that would be most affected by the presence of NO_x are shown based on NO concentration and provided in the Supporting Information, Figure S3. At NO concentration greater than 0.1 ppb, the delay seen in the CIMS measurement of the 1,4-hydroxycarbonyl is not reproduced (Supporting Information, Figure S3a). The 1,4-hydroxycarbonyl is an important intermediate in SOA formation in the presence of NO_x,[12,38] so the presence of NO should enhance its production and contribute to initial organic growth. The observed delay in the organic growth as measured by the AMS is consistent with the absence of any appreciable NO_x in the system. Further, the presence of NO should accelerate formation of the hydroxy hydroperoxide (OHROOH) (Supporting Information, Figure S3b), causing the simulations to further deviate from the observed gas-phase measurements. These analyses support the fact that residual NO_x does not play a significant role in the overall chemistry represented and that the majority of alkoxy radical formation is not a result of RO_2 + NO chemistry. In addition, CIMS spectra show no evidence of nitrate compounds formed. Thus, the

dx.doi.org/10.1021/jp211531h | J. Phys. Chem. A 2012, 116, 6211−6230

photochemical mechanism used in the remainder of this study excludes the presence of NO_x.

Hydroperoxide Photolysis. The OH-initiated reaction of dodecane results in the formation of the peroxy radical which, upon reaction with HO_2, rapidly produces the hydroperoxide ($C_{12}H_{26}O_2$, ROOH in Figure 1). The hydroperoxide can undergo further reaction with OH or photolyze. In the absence of an explicit photolysis rate, following MCM 3.2, the methyl hydroperoxide photolysis rate is used as a proxy for the photolysis rate of hydroperoxide species. Using absorption cross sections and quantum yields for methyl hydroperoxide (CH_3OOH)[39,40] with the actinic flux calculated from spectral irradiance measurements in the chamber using a LICOR spectroradiometer, the expected photolysis rate constant of methyl hydroperoxide is calculated to be $j = 2.30 \times 10^{-6}$ s^{-1}. Under these experimental conditions, the C_{12} hydroperoxide is simulated in the mechanism to react with OH and undergo photolysis in branching ratios of 86% and 14%, respectively. The most likely route of photolysis is to sever the O−OH bond rather than the C−OOH bond in the hydroperoxy group,[41] resulting in the formation of an alkoxy radical. In the domain of $RO_2 + HO_2$ chemistry, alkoxy radicals can be generated only via photolysis of a hydroperoxy group; there is no formation of simple alcohols, which is the same when NO_x is present.[9,11,14,15] Along Channel 3 of the mechanism in Figure 1, the hydroperoxide photolyzes to generate the alkoxy radical. Due to the length of the carbon chain, isomerization through a 1,5-hydride shift will occur,[9,11,15] generating a hydroxy group and leaving a radical on a secondary carbon. Reaction of this radical with O_2 followed by reaction with HO_2 leads to the hydroxy hydroperoxide ($C_{12}H_{26}O_3$) referred to as OHROOH in Figure 1, which can undergo photolysis or further reaction with OH. Under photolysis, the same reverse isomerization of the resulting hydroxy alkoxy radical occurs to form a 1,4-hydroxycarbonyl ($C_{12}H_{24}O_2$)[9,11] referred to as OHCARB in Figure 1. On the basis of the calculated photolysis rate constant of methyl hydroperoxide as a proxy and the OH concentration lumped reaction rate constant, $k_{OH} = 9.94 \times 10^{-5}$ s^{-1}, generation of the 1,4-hydroxycarbonyl (OHCARB) via reaction with OH is the preferred pathway. The 1,4-hydroxycarbonyl is estimated to react with OH and undergo photolysis in branching ratios of 98% and 2%, respectively, according to the photochemical simulation. In the case of reaction with OH, the positions of the carbonyl and hydroxy groups would be switched from what is shown in the mechanism. This formation mechanism of the 1,4-hydroxycarbonyl (OHCARB) is also distinct from the predominant reverse isomerization mechanism when in the presence of NO_x.[9,11,14,15] Still, an even quicker route of formation is through alkyl peroxy radical isomerization with an extrapolated isomerization rate constant of 0.03 s^{-1} at 298 K, which is applicable to the conditions of $[RO_2] < 6 \times 10^{12}$ molecules cm^{-3} and $[NO] < 3 \times 10^9$ molecules cm^{-3}.[15,42,43] Since the NO concentration is only confidently known to be <5 ppb or 1×10^{11} molecules cm^{-3} (the lower detection limit of our NO_x analyzer), the alkyl peroxy radical isomerization route is unconfirmed.

Hydroperoxide + OH. The hydroperoxide primarily reacts with OH, in which abstraction of the hydrogen from the hydroperoxy-containing carbon is favored.[41] This leads to decomposition of the hydroperoxy group to form a carbonyl ($C_{12}H_{24}O$), resulting in recycling of OH radical (Channel 1, CARB in Figure 1). In the case in which the OH attacks another secondary carbon along the hydroperoxide chain, a dihydroperoxide, $C_{12}H_{26}O_4$, (Channel 2 in Figure 1) may be formed. Reaction of the carbonyl or the dihydroperoxide with OH would generate the third-generation carbonyl hydroperoxide (CARBROOH), with chemical formula $C_{12}H_{24}O_3$. OH reaction with the carbonyl generally favors attack at a carbon beta from the existing carbonyl group;[34] however, a small fraction could occur at the α position. Depending on the relative positions of the carbonyl and hydroperoxy group, fragmentation or functionalization will occur. In the case of Channel 1, the carbonyl and hydroperoxy groups are on adjoining carbons, such that when photolysis of the hydroperoxy group generates the alkoxy radical, scission of this C−C bond is favored. Products along Channel 1a are referred to as p(jCARBROOH) in reaction 17 of Table 2. Decomposition of the carbonyl alkoxy radical leads to an acyl radical and an aldehyde. The eventual fate of the acyl radical is reaction with O_2 to generate an acyl peroxy radical, which reacts with HO_2 to generate acids (Channel 1a, CnCARBACID and CnACID) and eventually a shorter chain hydroperoxide (Channel 1a, CnROOH). While the formation of aldehydes and acids is reliant upon the formation of a less abundant form of the carbonyl hydroperoxide and its photolysis, Channel 1a serves an important role in generating aldehydes in a system with hydroperoxide species. These aldehydes can react in the particle phase to form PHAs, to be discussed later in the paper.

In the case of the carbonyl and hydroperoxy groups located beta to one another (Channel 2), photolysis (Channel 2a) or reaction with OH (Channel 2b) leads to more highly functionalized compounds than if the C_{12} backbone is fragmented as in Channel 1a. Products along Channel 2a are collectively referred to as p(CARBROOH + hν) in reaction 17 (Table 2), and products along Channel 2b are referred to as p(CARBROOH + OH) in reaction 16 (Table 2). In chemistry analogous to the photolysis route (Channel 3) of the initial hydroperoxide (ROOH), functionalization is achieved by gain of a hydroxy group through isomerization, leading to a multifunctional compound containing carbonyl, hydroxy, and hydroperoxide groups (Channel 2a). Again, the relative positions of these functional groups lead to hydroxy acids formation through photolysis (Channel 2ai, CnACID) or a 1,4-hydroxycarbonyl with an additional keto group (Channel 2aii). Consecutive OH reaction with the carbonyl hydroperoxide (CARBROOH) would lead to multiple keto groups forming from the previous hydroperoxide group (Channel 2b). However, the competitive photolysis of hydroperoxy groups leads to the variety in functionalization as in Channel 2a. Although the fate of the carbonyl hydroperoxide (CARBROOH) is likely to channel more carbon through reaction with OH (pCARBROOH + OH), (Channel 2b), the gas-phase chemistry in Channel 1a becomes important for SOA growth and will be discussed subsequently.

COMPARISON OF GAS-PHASE MECHANISM AND MEASUREMENTS

The dodecane−OH mechanism derived from the MCM 3.2[32,33] (Table 2) was used to simulate the first four generations of chemistry. The simulated hydrocarbon decay agrees with GC-FID measurements of dodecane in Figure 2a. The photolysis rate for H_2O_2 was calculated using the absorption cross section and quantum yield[39,40] with the chamber actinic flux, analogous to the calculation done for hydroperoxide species. The simple labels for compounds in Figure 1 are also used in the legend entries for the photochemical mechanism

and CIMS measurements comparisons throughout Figure 2. CIMS traces are referred to with a polarity as "(+)" or "(−)" preceding the m/z solely to indicate the ionization mode used, positve or negative, respectively. Table 3 provides a summary of the monitored CIMS ions and their suggested assignments.

Table 3. Signals Monitored by CIMS and Their Suggested Assignments

mode	m/z (s)	assignment	molecular formula
(−)	287	ROOH	$C_{12}H_{26}O_2$
(+)	223	CARB	$C_{12}H_{24}O$
(+)/(−)	204/301[a]	CARBROOH	$C_{12}H_{24}O_3$
(+)/(−)	206/303[a]	OHROOH	$C_{12}H_{26}O_3$
(−)	285	OHCARB	$C_{12}H_{24}O_2$
(−)	315[a]	DICARBROOH	$C_{12}H_{22}O_4$
(−)	317[a]	OHCARBROOH	$C_{12}H_{24}O_4$
(−)	187	C5CARBACID	$C_5H_{10}O_2$
(−)	135/201	C6CARBACID	$C_6H_{12}O_2$
(−)	149/215	C7CARBACID	$C_7H_{14}O_2$
(−)	163/229	C8CARBACID	$C_8H_{16}O_2$
(−)	177/243	C9CARBACID	$C_9H_{18}O_2$
(−)	191/257	C10CARBACID	$C_{10}H_{20}O_2$
(−)	205/271	C11CARBACID	$C_{11}H_{22}O_2$
(−)	203	C5ACID/C6ROOH	$C_5H_{10}O_3/C_6H_{14}O_2$
(−)	151/217	C6ACID/C7ROOH	$C_6H_{12}O_3/C_7H_{16}O_2$
(−)	165/231	C7ACID/C8ROOH	$C_7H_{14}O_3/C_8H_{18}O_2$
(−)	245	C8ACID/C9ROOH	$C_8H_{16}O_3/C_9H_{20}O_2$
(−)	193/259	C9ACID/C10ROOH	$C_9H_{18}O_3/C_{10}H_{22}O_2$

[a]Denotes negative mode ions at m/z > 300 monitored in the January 18 h experiment. All other m/z's were monitored in the January and March experiments.

The mechanism was used primarily for evaluating time profiles of expected products in the CIMS measurements. The scales for the CIMS signal and the simulated output have been adjusted for peak matching to compare the trends in Figure 2. Reduced χ^2 values are given for the fit of the simulated trace and the CIMS measurements using the maximum value for the first 18 h as the normalization parameter. The χ^2 for the simulated and measured 1,4-hydroxycarbonyl (OHCARB) is for the first 18 h since the measurement decays, but the simulation does not include a reactive sink. Vapor-phase wall loss is not treated here in the photochemical model or in correcting the gas-phase observations (for reasons described in the Experimental Section), although it is likely to play a role affecting the more highly oxidized lower volatility products formed as in other chamber studies.[44,45] While the gas-phase chemistry represented in the mechanism generally describes the gas-phase CIMS trends for many species such as the hydroperoxide (ROOH), carbonyl (CARB), and carbonyl hydroperoxide (CARBROOH), the hydroxy hydroperoxide (OHROOH) may be subject to greater vapor-phase wall loss, contributing to some of the discrepancy between the simulated and measured trace in the begininng of the experiment. This effect is discussed further in the following section.

Mechanism and Measurement Comparison of Hydroperoxide + OH. Mechanism predictions of the hydroperoxide (ROOH) capture the trend of the CIMS measurements for the hydroperoxide (−) m/z = 287 (Figure 2b). At its peak, the hydroperoxide is simulated to represent about 20% of the initial carbon. While the hydroperoxide production rate is captured by the ROOH photochemical mechanism, the simulated loss is overestimated. The loss processes for the hydroperoxide include ROOH + OH and ROOH + hν. As noted, the MCM 3.2 gives an explicit reaction rate constant for a C_{12} hydroperoxide with OH, but utilizes the photolysis rate of CH_3OOH as a general photolysis rate for all hydroperoxide species. Extrapolating the photolysis rate from a C_1 to a C_{12} hydroperoxide is a source of uncertainty in the simulated trace. The simulated chemistry is more rapid than the measurements, consistent with a faster than measured production rate of the carbonyl.

The MCM 3.2 mechanism for dodecane does not include explicit reactions for formation of the dihydroperoxide (Channel 2), although evidence exists in the CIMS data at (−) m/z = 319 (CF_3O^- cluster) that suggests formation. The possibility of alkyl peroxy radical isomerization[46] was also considered, but this is unlikely under these experimental conditions because the [HO_2] and [OH] are not low enough to extend the lifetime of the alkyl peroxy radical for it to isomerize. Because the carbonyl (CARB) is not sufficiently polar to be detected in the negative mode ionization, it was monitored in positive mode at (+) m/z = 223. The carbonyl measurements also track the mechanism simulations, although with a slight lag (Figure 2c). The carbonyl (CARB) forms quickly, simultaneously with the hydroperoxide generation, so its peak just after 10 h represents almost a third of the initial carbon. The carbonyl hydroperoxide (CARBROOH) monitored at (+) m/z = 204 also times well with the model output during growth, but the gas-phase concentration remains low overall because of its many reactive sinks.

Owing to the complexity of the many later generation products, these are not represented explicitly in the mechanism, and the simulation terminates with the remaining carbon represented in further reaction of the carbonyl hydroperoxide. This includes three possible routes as discussed previously and seen in Figure 1: (1) photolysis and subsequent decomposition if the carbonyl and hydroperoxy group are vicinal (Channel 1a), (2) photolysis of the hydroperoxy group beta to the carbonyl (Channel 2a), and subsequent decomposition products (Channel 2ai) or C_{12} retaining products (Channel 2aii), and (3) continued OH reaction and functionalization of the C_{12} molecule (Channel 2b). The respective photolysis of the α-carbonyl hydroperoxide (Channel 1a) and the β-carbonyl hydroperoxide photolysis (Channel 2a) or reaction with OH (Channel 2b) are represented in the mechanism scheme in Figure 1. However, the MCM 3.2 makes no distinction between reaction rates for isomers of the carbonyl hydroperoxide, so the sum of the α-carbonyl hydroperoxide (Channel 1) and the β-carbonyl hydroperoxide (Channel 2) are implemented in the photochemical simulation as (CARBROOH). Thus, the subsequent photolysis product from the α-carbonyl hydroperoxide (Channel 1a) and the β-carbonyl hydroperoxide (Channel 2a), respectively, will produce the same time trend from the photochemical simulation (Table 2, Reaction 17), although we distinguish the alpha photolysis products (Channel 1a) as p(jCARBROOH) and the beta photolysis products (Channel 2a) as p(CARBROOH + hν) for relevant discussion on a distinct set of products formed from photolysis of each isomer. That is, acid formation (Figures 3b and 4b) is considered as p(jCARBROOH), and the multifunctional formed via Channel 2a is considered as p(CARBROOH + hν) in Figure 2e.

Note that photolysis of the β-carbonyl hydroperoxide (Channel 2ai) produces a hydroxy carbonyl hydroperoxide

dx.doi.org/10.1021/jp211531h | J. Phys. Chem. A 2012, 116, 6211−6230

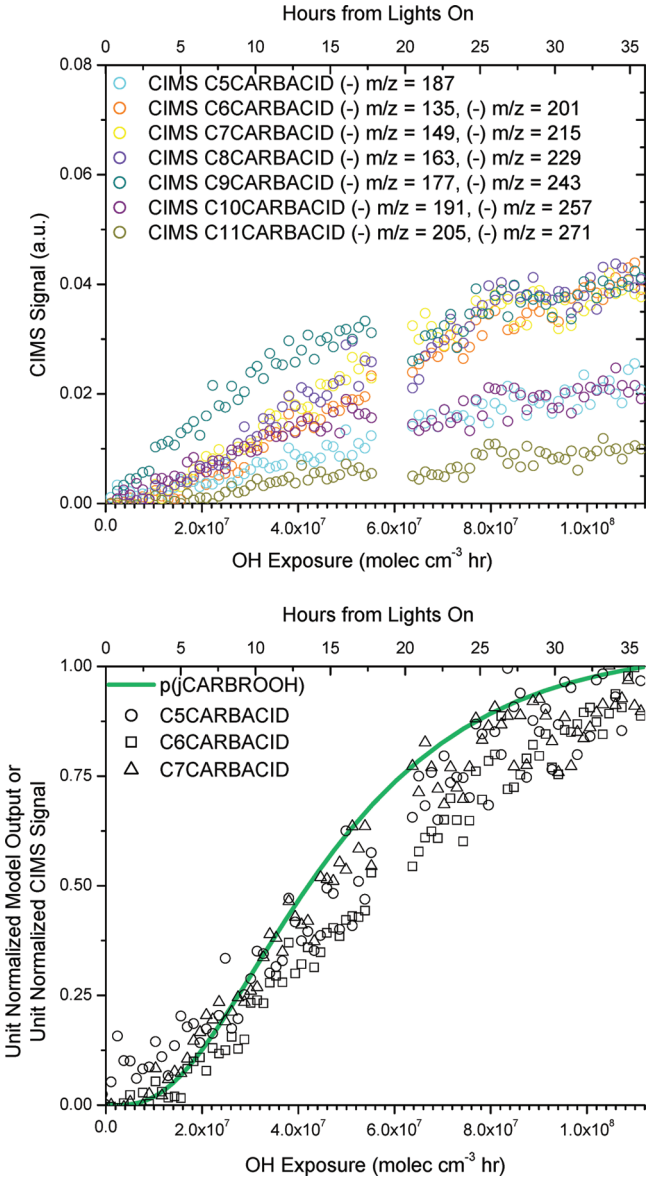

Figure 3. Carboxylic acids. (a) Series of suggested C_5 through C_{11} carboxylic acid traces and the ions measured in CIMS negative mode ionization. (b) Representative C_5 through C_7 carboxylic acid traces on a unit normalized scale trend with modeled results for photolysis of the carbonyl hydroperoxide.

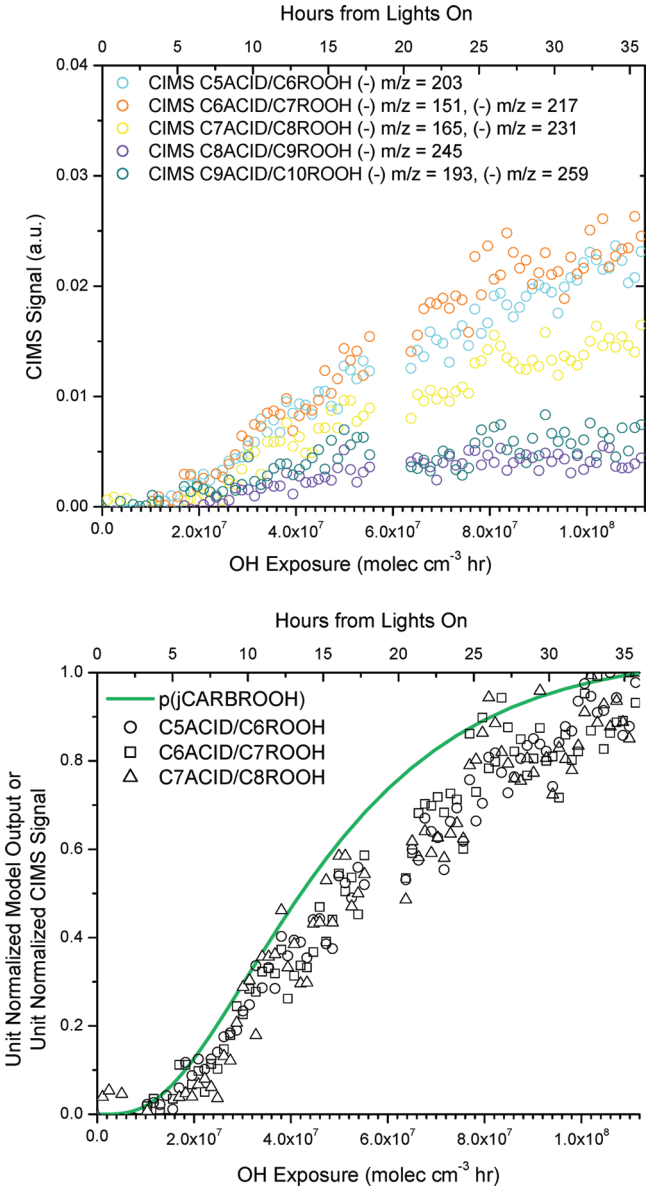

Figure 4. Acids (hydroxycarboxylic/peracid) or hydroperoxides. (a) Series of suggested C_5 through C_9 peracid and hydroxy carboxylic acid, and C_6 through C_{10} hydroperoxide traces. Since the peracid and hydroxy carboxylic acid are the same molecular weight as a hydroperoxide with one additional carbon, the ions measured by the CIMS may have contributions from all three species. (b) Example unit normalized trends of C_5 through C_7 peracids and hydroxycarboxylic acids, and C_6 through C_8 hydroperoxides that trend with the product of carbonyl hydroperoxide photolysis from the mechanism.

(OHCARBROOH) with the carbonyl and hydroperoxide groups vicinal. Photolysis of this multifunctional compound shows a parallel decomposition route to Channel 1a leading to hydroxy acids. Channel 2aii retains the C_{12} backbone, because, although it also starts with a hydroxy carbonyl hydroperoxide (OHCARBROOH), the carbonyl and hydroxy functional groups are nonvicinal to the −OOH group. Analogous to the treatment of the two carbonyl hydroperoxide (CARBROOH) isomers, these two hydroxy carbonyl hydroperoxide (OHCARBROOH) isomers are also not distinguished in the photochemical simulation; they are shown as p(CARBROOH + hν). That is, Figure 2e compares the simulated output of p(CARBROOH + hν) to the CIMS measured ion suggested for the multifunctional compound (presumably OHCARBROOH, $C_{12}H_{24}O_4$) at (−) m/z = 317 to represent Channel 2a. Products of the continued OH oxidation of the β-carbonyl hydroperoxide (Channel 2b) are simulated under p(CARBROOH + OH), which has a distinct output from that of the carbonyl hydroperoxide photolysis, represented identically in p(CARBROOH + hν) and p(jCARBROOH). Production of a possible dicarbonyl hydroperoxide (presumably DICARBROOH, $C_{12}H_{22}O_4$), monitored at (−) m/z = 315, represents this channel in the mechanism (Channel 2b). Note that the signals at (−) m/z = 317 and (−) m/z = 315 do not extend the full 36 h because they were not monitored for a full 36 h as described in the Experimental Section. More detailed treatment of Channel 1a is discussed subsequently relative to acid formation.

dx.doi.org/10.1021/jp211531h | J. Phys. Chem. A 2012, 116, 6211−6230

Mechanism and Measurement Comparison of Hydroperoxide Photolysis. The hydroxy hydroperoxide measurements exhibit the largest deviation of all CIMS traces from the simulated hydroxy hydroperoxide (OHROOH) (Figure 2f). While we cannot fully account for this discrepancy at the present time, it could be possible that (1) the hydroxy hydroperoxide formation is in fact slower than predicted by using the photolysis rate of a C_1 hydroperoxide for the C_{12} hydroperoxide and (2) the hydroxy hydroperoxide (OHROOH) has sufficiently low volatility that it may be lost to the chamber walls more quickly than other gas-phase compounds. We observe that the chemistry in general is actually slower than the simulation. That is, the simulated hydroperoxide (ROOH) exhibits a faster decay than that of the measurement (Figure 2b) and subsequent products (CARB, CARBROOH, and OHROOH) are simulated to rise more quickly than their individual measurements (Figure 2c,d,f). Hence, we do expect that OHROOH's actual rise will come later than that simulated. If gas-to-wall partitioning is responsibile for the discrepancy, the walls may first act as a reservoir but subsequently release the hydroxy hydroperoxide back to the gas-phase as it is removed by secondary reactions, shifting the trend of the gas-phase measurement from the simulated trend. We return to the hydroxy hydroperoxide sinks in the SOA Growth section.

The 1,4-hydroxycarbonyl (OHCARB, Figure 2g) is generated from the hydroxy hydroperoxide (OHROOH, Figure 2f) in greater concentration than its precursor. As discussed earlier, the 1,4-hydroxycarbonyl may be formed via photolysis of the hydroxy hydroperoxide (OHROOH + hν) or via hydroxyl radical reaction with the hydroxy hydroperoxide (OHROOH + OH). The relative contributions from these sources to 1,4-hydroxycarbonyl (OHCARB) formation are shown in Figure 2g. The CIMS measurement of the 1,4-hydroxycarbonyl at (−) m/z = 285 follows the simulated production despite discrepancy in the simulation and measurement for its precursor, the hydroxy hydroperoxide (OHROOH). This may suggest that the true time profile for OHROOH is not captured by the measurement. The vapor pressure of OHROOH is about 2 orders of magnitude lower than OHCARB, so one hypothesis is that the early losses of OHROOH are due to vapor-phase wall loss to the reactor walls and reaction with OH to form OHCARB. Mass closure is needed to confirm whether the measurements match the expected OHROOH distribution among losses to the wall and its oxidation to OHCARB, but it is possible that if the OHROOH is converted quickly to OHCARB via reaction with OH (lifetime ∼ 2.8 h), then the trend in the CIMS measurement for OHCARB would still agree with the simulation early on as observed (Figure 2g). Although there is no explicitly simulated sink for the 1,4-hydroxycarbonyl (OHCARB), the measurement peaks sometime after 18 h. It is expected that from the difference between the gas-phase and mechanism trends, roughly 0.3 ppb of it exists in this sink.

Mechanism and Measurement Comparison of Acid Formation. Acidic species are expected to form from photolysis of a hydroperoxy group that is vicinal to another oxygen containing carbon. Photolysis of the hydroperoxy group results in an alkoxy radical vicinal to another oxygen containing carbon so decomposition ensues (see Figure 1, Channels 1a and 2ai). Depending on where in the molecule the C−C bond is severed, varying carbon length carboxylic acids (Channel 1a, CnCARBACID, $C_nH_{2n}O_2$), peracids (Channel 1a, CnACID, $C_nH_{2n}O_3$), hydroxycarboxylic acids, (Channel 2ai, CnACID $C_nH_{2n}O_3$), and hydroxyperacids (Channel 2ai) result. Such compounds in the CIMS may appear as both the transfer (m/z = $[M + 19]^-$) and the cluster product (m/z = $[M + 85]^-$), so the traces shown are the sum of these two ions (see Figure 3 and Figure 4). In some cases, like the C_5 carboxylic acid, there were additional contributions to the cluster product ion (m/z = 253), so it is omitted. The C_9 carboxylic acid likely has contributions from an unidentified mass interferent since its time profile is slightly different than the others. The overall time profiles and their relative abundances are consistent with expectations that C_{11} acid production is least likely to form, as tertiary H abstraction at the end carbons is slower.[34] Still, distribution by carbon number would need to be confirmed after full mass quantification. When unit normalized, the carboxylic acid traces (CnCARBACID) collapse to a distinct time profile consistent with the modeled trace representing the photolysis products of the carbonyl hydroperoxide p-(jCARBROOH) in Figure 3b.

The formation of a peracid (Channel 1a, CnACID) of the same carbon number as a hydroxy carboxylic acid (Channel 2ai, CnACID) is difficult to discern, as they are isomers. Thus, these two types of acids have been referred to generally as CnACID, and this is separate from the carboxylic acids referred to as CnCARBACID. Other isomers include a hydroperoxide (Channel 1a, CnROOH) with an additional carbon. Hence, the ions monitored are generally assigned as a C_n acid or a C_{n+1} hydroperoxide in Figure 4. Still, it is more likely that the majority initial contribution to these ions stems from the peracid, as the hydroxycarboxylic acid (Channel 2ai, CnACID) is a higher generation product. Further, resulting branching ratios for the products of the acyl peroxy radical reaction with HO_2, as discussed in Hasson et al.[47] for the case of acetyl peroxy radical ($CH_3C(O)O_2$), would tend to favor peracid (via $R(O)O_2 + HO_2 \rightarrow R(O)OOH$) and carboxylic acid formation (via $R(O)O_2 + HO_2 \rightarrow R(O)OH + O_3$) routes over generation of another alkoxy radical (leading to the eventual < C_{12} hydroperoxides of Channel 1a in the dodecane case). Again, on a unit normalized basis, these ion traces collapse onto the unit normalized mechanism prediction for the products of carbonyl hydroperoxide photolysis, p(jCARBROOH), consistent with this identification as peracids accompanying carboxylic acid formation (Figure 4b). While the decomposition products (i.e., acyl radical and aldehyde) in Channel 1a preceding acid formation are not explicitly modeled, the reaction of the acyl radical with O_2 is considered instantaneous, and the lifetime of an acyl peroxy radical with HO_2 is expected to be 3.7 s under low-NO_x conditions. Thus, comparison of the acid traces with p(jCARBROOH) is sufficiently close for comparison to the trend in the gas-phase measurements. While the aldehydes could not be explicitly monitored by the CIMS, the acid traces are confirmation of aldehyde formation in the gas-phase. The aldehyde will be seen to be an important gas-phase intermediate, for its role in PHA formation.

Carbon Balance. Now we discuss the fate of the initial mass of dodecane distributed among the various reaction channels in the mechanism and compare to the gas-phase measurements. More reactions are represented in the mechanism scheme of Figure 1 than are implemented in the photochemical simulation (Table 2). While the distinct product distribution from photolysis of the two isomers of the carbonyl hydroperoxide (CARBROOH) matters for the gas-phase chemistry and SOA formation, the alpha isomer is not

considered in MCM 3.2, although reactions along Channel 2a including the formation and fate of a hydroxy carbonyl hydroperoxide (OHCARBROOH) are included. As is, the photolysis rates of the carbonyl hydroperoxide (CARBROOH) isomers would be treated the same, so p(jCARBROOH) and p(jCARBROOH + hν) are simulated to be the same (Table 2, Reaction 17). This prevents further explicit extension of the photochemical simulation for products along Channel 1a without further approximation of reaction rate coefficients. For carbonyl hydroperoxide (CARBROOH) reaction with OH, MCM 3.2 ends with production of the carbonyl hydroperoxy radical ($CARBRO_2$ in reactions 13 and 14 of Table 2); $CARBRO_2$ then goes back to the carbonyl hydroperoxide (CARBROOH) after reaction with HO_2 for these experimental conditions. That is, MCM 3.2 does not suggest further oxidation of CARBROOH to a dicarbonyl or to a thrice-functionalized chain (DICARBROOH), as supported by the CIMS trace monitored at (−) m/z = 315 (DICARBROOH). Effectively, this route (Channel 2b) becomes a large carbon sink without further explicit treatment of the products. With the limitation of measurable gas-phase species beyond this point, extension of the photochemical simulation is not attempted, although the further extent of oxidation is of interest, as it will play a role in the volatilities of products and contribution to particle growth.

The simulated fraction of initial carbon over time in the various generations of products is shown in Figure 2h. After sufficient time, the majority of the carbon resides in fourth and later generation products. While fourth and later generation products represent over half of the initial carbon, the major development of this chemistry becomes apparent after the third and earlier generations peak around 2.3×10^7 molecules cm^{-3} h of total OH exposure (~10 h). This would correspond to almost a day of atmospheric aging, assuming an ambient OH concentration of $\sim 10^6$ molecules cm^{-3}. Thus, dodecane and other alkanes that have similarly long OH-reactive lifetimes have the potential for generating multifunctional semivolatile species over the course of a few days.

Although CIMS sensitivities to each individual compound could not be determined (see Experimental Section), we used previously determined sensitivities for compounds with similar functionality as proxies for the sensitivity of species in this mechanism. We used the previously measured sensitivity of methyl hydroperoxide (CH_3OOH)[23] for the C_{12} hydroperoxide monitored at (−) m/z = 287, and the previously measured sensitivity of hydroxyacetone ($C_3H_6O_2$)[48] for the acids and multifunctional compounds. At the end of 18 h, it is estimated that roughly 13 ppb within a factor of 2 of the simulated 31 ppb of dodecane reacted is accounted for by the CIMS negative mode ions measured. All CIMS traces shown in Figure 2 were included, except the carbonyl (CARB, Figure 2c), as it could only be monitored in positive mode, and signal intensities of this mode are not comparable to that of negative mode. Although the carbonyl hydroperoxide (CARBROOH, Figure 2d) and the hydroxy hydroperoxide (OHROOH, Figure 2f) are tracked in positive mode over 36 h, we used the signals at (−) m/z = 301 and (−) m/z = 303, respectively, from the 18 h January experiment for a rough carbon balance at 18 h. The acid traces shown in Figure 3a and Figure 4a were also included, although there is likely a great deal of carbon still unaccounted for in < C_5 acids. Other remaining carbon not accounted for by the CIMS measurements include vapor-phase wall loss (though it is expected to be small), aldehyde formation from Channel 1a of the mechanism, and the many later generation products along Channel 2 that are not explicitly monitored by the CIMS.

SOA GROWTH

Organic growth as measured by the AMS is shown versus the dodecane decay in Figure 2a. The AMS organic trace is not corrected for particle wall-loss. The onset of growth occurs coincident with the peak of the hydroperoxide, indicating aerosol formation from higher generation oxidation products. The total suspended particle organic peaked at approximately 63 $\mu g\ m^{-3}$ around hour 20, consistent with the development of fourth-generation gas-phase chemistry. Peak particle diameter grew from 58 nm (seed diameter) to 190 nm at the point of maximum concentration, and then to 200 nm by the end of the experiment as measured by the DMA. Further analyses and consideration of heterogeneous chemistry provide more insight into the dynamics of the aerosol growth.

Vapor Pressure Estimation. To better constrain the expected aerosol chemical makeup, vapor pressures at 298 K were estimated for an array of compounds listed in Table S2 of the Supporting Information section using the EVAPORATION (Estimation of Vapor Pressure of ORganics, Accounting for Temperature, Intramolecular, and Nonadditivity effects) method.[49] The method predicts the (subcooled) liquid pure compound vapor pressure, p^0, taking into account intramolecular effects from the positions of functional groups on a compound. For example, the predicted p^0 for the α-carbonyl hydroperoxide is 6.58×10^{-8} atm, more than twice that of the β-carbonyl hydroperoxide, $p^0 = 2.45 \times 10^{-8}$ atm. Conversion of the pure component liquid vapor pressure to a value of C_i^o in units of $\mu g\ m^{-3}$ (also in Table S2, Supporting Information) can be used to classify compounds according to previously defined volatility classes.[50] These classes in order of increasing volatility include extremely low volatility organic compounds (ELVOCs) with $C_i^* < 3 \times 10^{-4}\ \mu g\ m^{-3}$, low volatility organic compounds (LVOCs) with $3 \times 10^{-4} < C_i^* < 0.3\ \mu g\ m^{-3}$, semivolatile organic compounds (SVOCs) with $0.3 < C_i^* < 300\ \mu g\ m^{-3}$, intermediate volatility organic compounds (IVOCs) with $300 < C_i^* < 3 \times 10^6\ \mu g\ m^{-3}$, and finally volatile organic compounds (VOCs) with $C_i^* > 3 \times 10^6\ \mu g\ m^{-3}$. These volatility regimes are provided for reference in Figure 5. Note that the calculated values presented here are not the conventionally used C_i^*, since values for the activity coefficients, γ_i, are not estimated and experimental volatility measurements were not made. C_i^* is related to C_i^o through the activity coefficient, $C_i^* = \gamma_i C_i^o$.[50]

O:C Values. The O:C values for each molecule are included in the Supporting Information section, Table S2. To view the progression of the oxidation, each compound is shown in the O:C versus log C_i^o space (Figure 5). The marker colors indicate the gas-phase generation of the compound. Black markers are reserved specifically for those compounds that may participate in heterogeneous chemistry. Each compound has a letter assigned label, corresponding to the key used in Table S2. A general upward trend to the left indicates lower volatility and increasing oxygenation over time. Exceptions do occur where there is formation of second generation compounds, like the hydroxy hydroperoxide and the dihydroperoxide, of a higher O:C and lower volatility compared to later generation products. AMS measurements show that within the first 10 h of early growth, the O:C stabilizes at 0.22, after which it steadily increases to 0.30 by the end of the experiment. O:C measurements are estimated to have an uncertainty of 30%,[51]

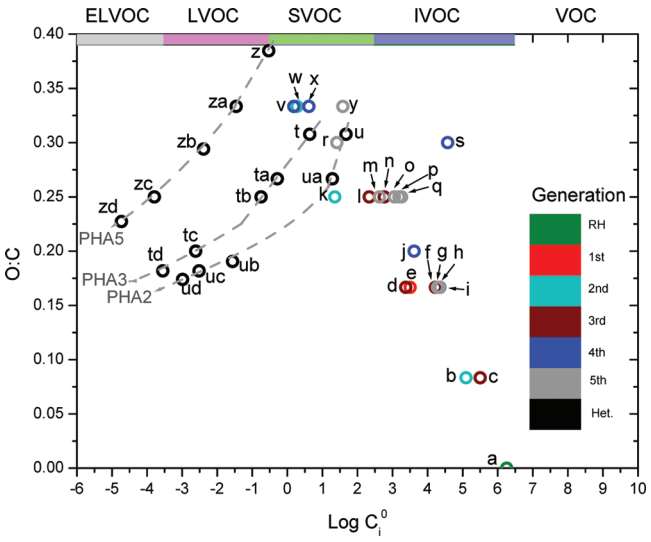

Figure 5. Span of O:C values versus log of the pure subcooled liquid vapor pressures in units of μg m^{-3} (C_i^o) for predicted compounds from dodecane low-NO$_x$ photoxidation. Colored markers indicate the product generation, and black markers indicate compounds thought to participate in heterogeneous chemistry. Letter data labels correspond with the compounds listed in Table S2. Regions of volatility previously defined[50] are denoted along the top axis for reference. The overall progression is upward to the left; vapor pressure drops from the starting dodecane, "a", at log(C_i^o) = 6.3 to log(C_i^o) = 0.19 for $C_{12}H_{24}O_4$, "v", and O:C increases to a max at 0.33. AMS measured O:C of 0.22−0.30 during the experiment. The gray dashed lines indicate the progression of increasing carbon length on the aldehyde that reacts with a hydroperoxy compound to form PHAs. PHA2 represents formation of the carbonyl hydroperoxide (CARBROOH) derived PHA, γ-keto-α-alkyl-α'-hydroxyalky peroxide (KAHAP); PHA3 the hydroxy hydroperoxide (OHROOH) derived PHA, δ-hydroxy-α-alkyl-α'-hydroxyalky peroxide (HAHAP); and PHA5 the hydroxycarbonyl hydroperoxide derived PHA, ε-hydroxy-γ-keto-α-alkyl-α'-hydroxyalky peroxide (HKAHAP). Increasing carbon length leads to convergence to a lower O:C and lower vapor pressure approaching the ELVOC region.

and the species shown in Figure 5 fall within the measured O:C range. The fifth-generation compounds in gray markers represent an increase in vapor pressure, owing to the formation of the hydroxy acids (Channel 2ai) and conversion of hydroperoxy groups to carbonyl groups. Only C_{10} acids are shown to condense the space and represent the bulk aerosol character. With estimated volatilities of expected gas-phase products and the measured O:C range, we investigate further the role of the semivolatiles on SOA growth.

Peroxyhemiacetal Formation. Many of the semivolatiles in Figure 5 are hydroperoxide species including (1) the second-generation hydroxy hydroperoxide (OHROOH, Channel 3; Figure 5 "k"), (2) the third-generation carbonyl hydroperoxide (CARBROOH, Channels 1 and 2; Figure 5 "n" and "l"), (3) the fourth-generation hydroxycarbonyl hydroperoxide (OH-CARBROOH, Channel 2a; Figure 5, "v" and "x"), and (4) the fifth-generation dicarbonyl hydroperoxide (DICARBROOH, Channel 2b; Figure 5, "y"). Once these semivolatiles have partitioned into the particle phase, reaction with aldehydes generated from decomposition of the photolyzed α-carbonyl hydroperoxide (Channel 1a) can occur to form PHAs. A general mechanism summarizing some possible reactions for the current system is shown in Figure 6. If the first-generation hydroperoxide (ROOH) reacts with an aldehyde, an α-alkyl-α'-hydroxyalky peroxide (hereafter referred to as AHAP) will be generated. If the β-carbonyl hydroperoxide (CARBROOH) reacts with an aldehyde, a γ-keto-α-alkyl-α'-hydroxyalky peroxide is formed (hereafter referred to as KAHAP). Similarly, if a hydroxy hydroperoxide (OHROOH) reacts with an aldehyde, a δ-hydroxy-α-alkyl-α'-hydroxyalky peroxide (hereafter referred to as HAHAP) will be formed. If a dicarbonyl hydroperoxide (DICARBROOH) reacts with an aldehyde, a ε-γ-diketo-α-alkyl-α'-hydroxyalky peroxide is formed (hereafter referred to as DKAHAP). Finally, if a hydroxycarbonyl hydroperoxide (OHCARBROOH) reacts with an aldehyde, a ε-hydroxy-γ-keto-α-alkyl-α'-hydroxyalky peroxide is formed (hereafter referred to as HKAHAP). There is also the possibility of cyclization of the KAHAP, DKAHAP, or HKAHAP because of the carbonyl groups, similar to the mechanisms proposed in previous studies,[52−54] although being isomers the cyclic and noncyclic forms would be hard to distinguish. Of course, alternative functional group placement on the compounds presented in Figure 6 is expected, and the compounds shown are examples.

PHA volatility will depend on the length of the aldehyde that originally reacted with the particle-phase incorporated hydroperoxide. Progression of the O:C and volatility of three select PHAs with increasing length of the aldehyde is marked by the series of "t" through "td" markers for HAHAP, "u" through "ud" for KAHAP, and "z" through "zd" for HKAHAP in Figure 5. The gray dotted lines are intended to guide the eye along these progressions toward lower O:C and lower vapor pressure, labeled "PHA2" for the KAHAP, "PHA3" for the HAHAP, and "PHA5" for the HKAHAP for visual clarity. PHA formation effectively converts semivolatiles into lower volatility products that approach the ELVOC region.

Evidence of PHA Formation Comparing Gas-Phase and Particle-Phase Mass Spectra. PHA formation is complex, as it involves reaction of a fourth-generation aldehyde (of varying carbon length) with second- to fifth-generation but lower vapor pressure hydroperoxy compounds at/in the particle. Figure 7 shows that aerosol growth follows after gas-phase formation of the carbonyl hydroperoxide (CARBROOH, Channels 1 and 2), but more importantly it is delayed until photolysis of the carbonyl hydroperoxide, p(jCARBROOH). The aldehydes could not be measured directly with CIMS because of their nonpolar nature, but the simulated p(jCARBROOH) can be used as a proxy for their expected formation according to Channel 1a in the mechanism. The aldehydes would precede acid formation, which is very quick after photolysis of the carbonyl hydroperoxide, when comparing the C_6CARBACID trace with the p(jCARBROOH) trace in Figure 7. From the trends presented in Figure 7, it appears that aerosol growth is timed with aldehyde formation, making PHA formation a potential mechanism for aerosol growth. This is further supported in species-specific comparisons of the CIMS and AMS.

Comparisons of the gas-phase mechanism predictions and CIMS traces were made with selected ion fragments from the HR-ToF-AMS mass spectra. The AMS utilizes vaporization and electron impact (EI) ionization resulting in fragmentation of aerosol species, but the prevalence of high amu (m/z > 100) in the spectra suggests that some stable high MW ions retain more of the original backbone and functionality of the initial product molecule. The selected ions discussed are those that would result from a PHA severed at either C−O bond of the peroxide RC_1−OO−C_2R. Scission at C_1−O results in the ion RC_1^+.

dx.doi.org/10.1021/jp211531h | J. Phys. Chem. A 2012, 116, 6211−6230

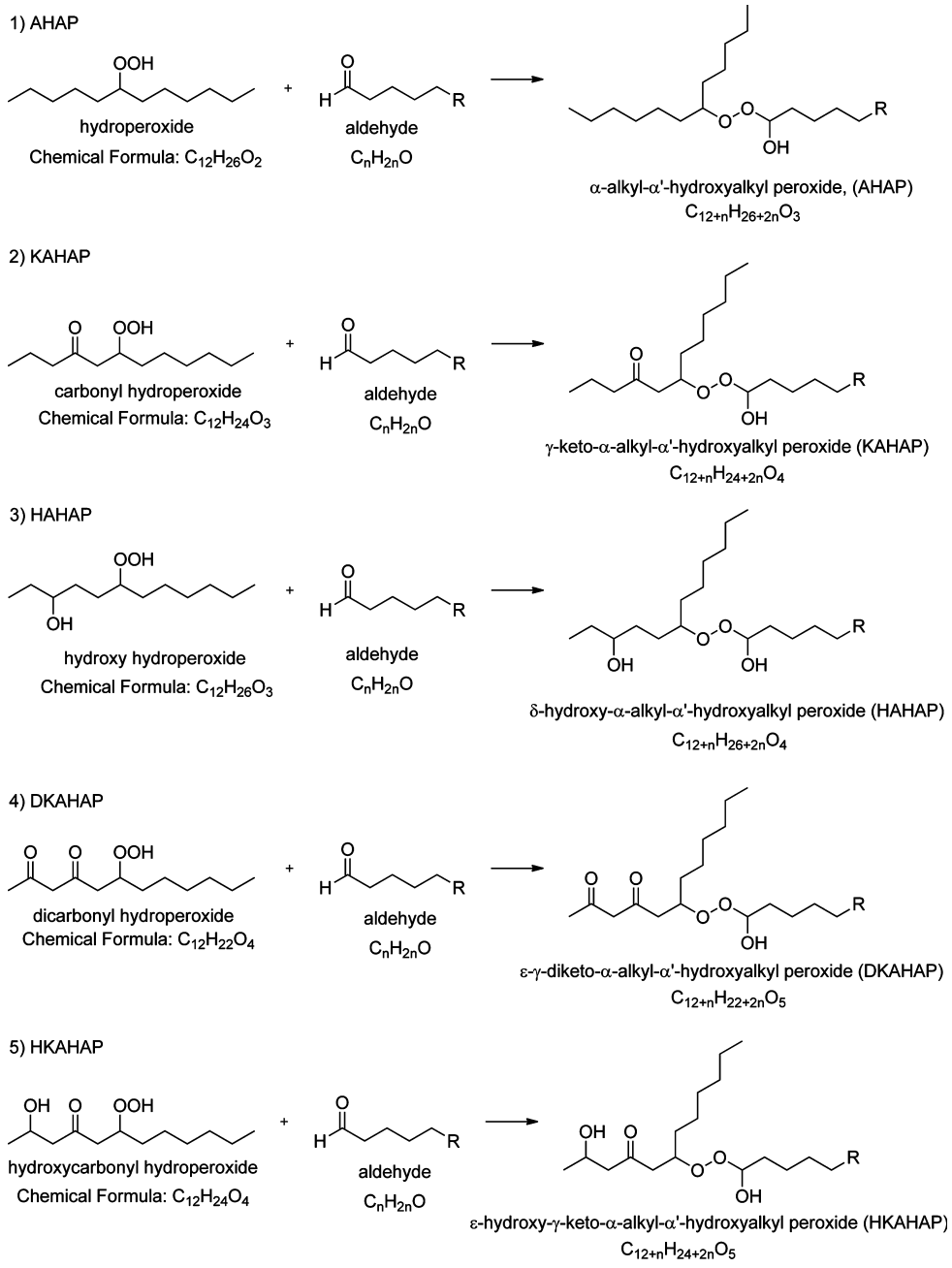

Figure 6. Scheme for forming five types of PHAs from reaction of an aldehyde of carbon length *n*, with various hydroperoxy compounds. (1) Reaction with a hydroperoxide generates an AHAP. (2) Reaction with a *β*-carbonyl hydroperoxide forms a KAHAP. (3) Reaction with a hydroxy hydroperoxide generates a HAHAP. (4) Reaction with a dicarbonyl hydroperoxide forms a DKAHAP. (5) Reaction with a hydroxycarbonyl hydroperoxide forms a HKAHAP.

Scission at C_2-O results in the ion RC_1OO^+, 32 amu greater than the RC_1^+ ion. The RC_1^+ ion was observed in previous studies of *α*-substituted hydroperoxide-derived PHAs,[52,55] although not the RC_1OO^+, which we propose for the PHAs in this study. The hydroperoxides we discuss in this study are not *α*-substituted, which may be cause for the different fragmentation pattern. Note that the RC_1^+ ion would be the equivalent ion generated from a hydroperoxide compound, RC_1-OOH, by loss of the hydroperoxy group to generate the $m/z = [M\text{-}33]^+$ ion, where M = mass of the hydroperoxide, also previously observed.[52,55] This fragmentation pathway was observed in identifying the C_{18} hydroperoxide during the standard experiment described previously in the Experimental section. Examination of $[M\text{-}33]^+$ ions and their exact masses from this fragmentation pathway alone suggests incorporation of the gas-phase carbonyl hydroperoxide (CARBROOH), hydroxy hydroperoxide (OHROOH), and other multifunctional long chains (OHCARBROOH, DICARBROOH) into the aerosol phase. However, the predominance of their respective RC_1^+ ions trending closely with their respective RC_1OO^+ ions strongly supports that these compounds are incorporated into the aerosol phase via PHA formation. The following discussion focuses on the pairing of $m/z < 200$ ions and their $m/z > 200$ (+ 32 amu) counterparts. For simplicity, we refer to the nominal mass of an ion rather than its exact

dx.doi.org/10.1021/jp211531h | J. Phys. Chem. A 2012, 116, 6211−6230

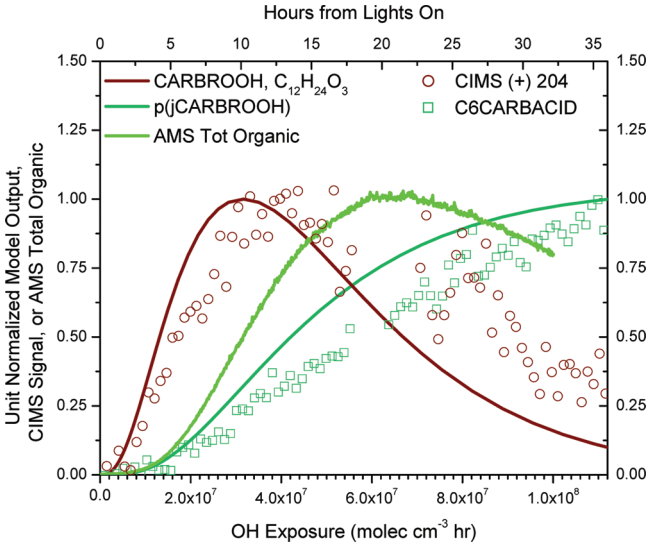

Figure 7. Aerosol growth occurs between formation of the carbonyl hydroperoxide (CARBROOH) and the onset of acid formation (observations in teal squares and simulated result, p(jCARBROOH), in teal) in the gas-phase. It is likely that initial aerosol growth can be supported by PHA formation since hydroperoxide containing species in the gas phase form within 5 h of lights on, and aldehyde formation will precede acid formation after photolysis of the carbonyl hydroperoxide.

mass, but the exact mass was used to obtain the chemical formula of the ion.

The AMS ions at m/z = 183 ($C_{12}H_{23}O^+$) and m/z = 215 ($C_{12}H_{23}O_3^+$) dominate the early SOA growth, suggesting that they may be characteristic fragments of the carbonyl hydroperoxide (CARBROOH)-derived PHA (KAHAP in Figure 6). Comparison of the simulated and measured gas-phase carbonyl hydroperoxide and AMS ions m/z = 183 and m/z = 215 is shown in Figure 8a along with the simulated gas-phase trend for photolysis of the carbonyl hydroperoxide, p(jCARBROOH) in Channel 1a. The growth of these ions in the aerosol phase is delayed from the onset of the carbonyl hydroperoxide formation in the gas phase until aldehyde formation begins, as proxied by the simulated p(jCARBROOH) trace in teal representing Channel 1a of the mechanism in Figure 1. As further reactions of the carbonyl hydroperoxide dominate, the gas-phase trace peaks and decays, followed as well by a decrease in these characteristic ions in the AMS mass spectrum. An analysis of the dynamics of the particle-phase AMS spectra will be addressed in a subsequent study.

AMS ions consistent with hydroxy hydroperoxide (OHROOH)-derived PHAs (HAHAP in Figure 6) at m/z = 185 ($C_{12}H_{25}O^+$) and m/z = 217 ($C_{12}H_{25}O_3^+$) grow in similarly with m/z = 183 and m/z = 215, although they peak later with their corresponding gas-phase trace (See Figure 8a and Figure 8b). Again, the appearance of these hydroxy hydroperoxide-derived PHA ions are contingent upon aldehyde formation as represented by the simulated p(jCARBROOH) trace in Figure 8b. If gas-to-particle partitioning was partially responsible for the simulated versus measured discrepancy for hydroxy hydroperoxide (OHROOH) Figure 2f, we would expect to see the m/z = 185 ion grow into the aerosol-phase before m/z = 217 and before aldehyde formation. That is, m/z = 185 growing in earlier to the aerosol-phase would indicate uptake of the hydroxy hydroperoxide (OHROOH) itself without conversion to PHA. With little SOA at this time and no aldehyde formation, partitioning of the hydroxy hydroperoxide early on is unlikely to account for this model-measurement discrepancy. It is possible that the hydroxy hydroperoxide lingers in the gas phase before aldehyde formation and undergoes vapor-phase wall loss as discussed previously.

The incorporation of the dicarbonyl hydroperoxide (DICARBROOH, $C_{12}H_{22}O_4$) into the particle phase is tracked with the AMS ion fragment at m/z = 197 ($C_{12}H_{21}O_2^+$) paired with m/z = 229 ($C_{12}H_{21}O_4^+$) in Figure 8c but after aldehyde formation. Note that, on a unit normalized scale, the p(jCARBROOH) overlaps the p(CARBROOH + OH) trend. This implies that dicarbonyl hydroperoxide (DICARBROOH) formation is practically simultaneous with aldehyde formation, although not necessarily in the same amount. The other thrice-functionalized chain, a hydroxycarbonyl hydroperoxide (OHCARBROOH, $C_{12}H_{24}O_4$) is tracked with AMS ion fragments m/z = 199 ($C_{12}H_{23}O_2^+$) and m/z = 231 ($C_{12}H_{23}O_4^+$). The ion trace at m/z = 199 is within the variation of the noisy CIMS marker at (−) m/z = 317 (Figure 8d).

Thus far, we observe that in the progression of increasing oxygenation (decreasing volatility) of the starting hydroperoxide there is less time between the gas-phase formation of a species and its incorporation into the particle phase. For example, there are a few hours between carbonyl hydroperoxide (CARBROOH) formation in the gas-phase measured by the CIMS at (+) m/z = 204 and the growth of the derived PHA AMS ions at m/z's 183 and 215 (Figure 8a). This is partially due to the delay in aldehyde formation. Still, once aldehyde is present, this time is significantly reduced for the delay between the hydroxy hydroperoxide (OHROOH) growth in the gas-phase measurement and its derived PHA ions (Figure 8b). While this also holds for the dicarbonyl hydroperoxide (DICARBROOH) in Figure 8c and the hydroxycarbonyl hydroperoxide (OHCARBROOH) in Figure 8d, there is a delay in the appearance of the AMS ions expected from their derived PHAs. That is, even though aldehyde is present and the thrice multifunctional compounds have been produced in the gas-phase, their incorporation as PHAs to the aerosol-phase is not timed with aldehyde formation as is the case for CARBROOH- and OHROOH-derived PHAs. This lag may be due to limiting reactant effects. That is, although the unit normalized simulations in Figure 8c suggest that DICARBROOH and aldehyde formation are practically simultaneous, it may be that the aldehyde produced is in lower quantity than the stoichiometric amount needed for reaction compared to the total semivolatile hydroperoxides available. Another possibility may be decreased reactivity of the dicarbonyl hydroperoxide (DICARBROOH) with another aldehyde since it already contains two carbonyl groups that may compete for or deactivate reaction with the hydroperoxy group, depending on their placement. Cyclization of carbonyl containing α-substituted hydroperoxides via intramolecular reaction of the carbonyl with the hydroperoxy group has been observed, setting up potential competition between cyclization and PHA formation.[52] Further study would be required to test for deactivation effects. Steric effects due to intramolecular hydrogen bonding[56] may also play a role for compounds like the hydroxy carbonyl hydroperoxide (OHCARBROOH). A previous study on the kinetics of α-hydroxy peroxides (RCH(OH)OOR) in solution noted that tetralin hydroperoxide is more reactive to acetaldehyde over cumene

dx.doi.org/10.1021/jp211531h | J. Phys. Chem. A 2012, 116, 6211−6230

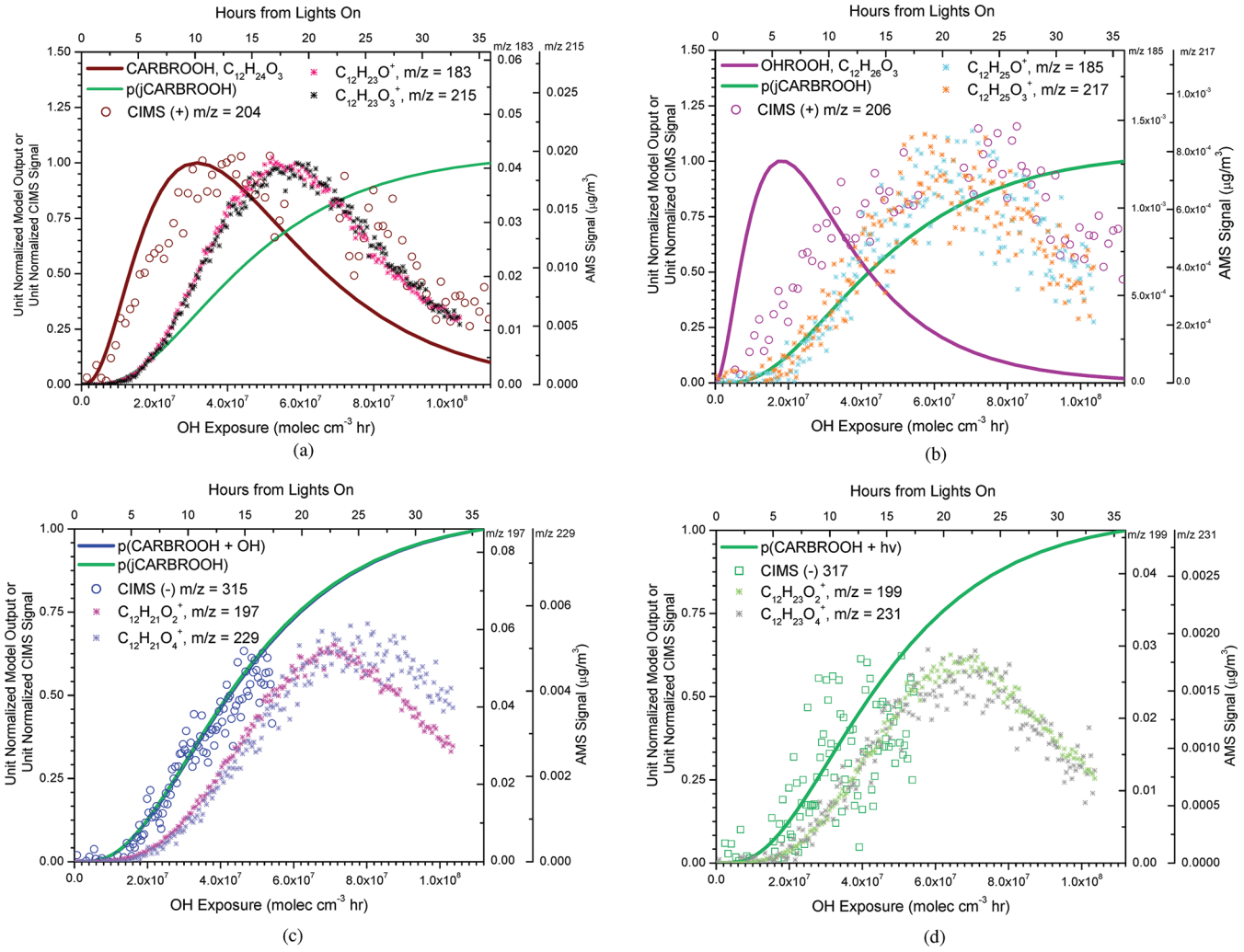

Figure 8. (a) AMS high-resolution fragments at m/z = 183 and m/z = 215 are possible characteristic fragments of the carbonyl hydroperoxide (CARBROOH)-derived PHA. (b) AMS high-resolution fragments at m/z = 185 and m/z = 217 are possible characteristic fragments of the hydroxy hydroperoxide (OHROOH)-derived PHA. (c) AMS high-resolution fragments at m/z = 197 and m/z = 229 are possible characteristic fragments of a multifunctional compound, dicarbonyl hydroperoxide (DICARBROOH)-derived PHA. (d) AMS high-resolution fragments at m/z = 199 and m/z = 231 are possible characteristic fragments of a multifunctional compound, hydroxycarbonyl hydroperoxide (OHCARBROOH) and its derived PHA.

hydroperoxide and other hydroperoxides because the peroxy group is surrounded by α-hydrogens.[56]

We note that the m/z = 183 and m/z = 185 (Figure 8a,b) ion fragments may be derived from other molecules containing similar functionalities to the carbonyl hydroperoxide (CARBROOH) and hydroxy hydroperoxide (OHROOH). For example, the fourth-generation hydroxycarbonyl hydroperoxide multifunctional (OHCARBROOH, Channel 2a) shares two of its functional groups with the carbonyl hydroperoxide (CARBROOH) and two with the hydroxy hydroperoxide (OHROOH), suggesting that there may be contributions to these ion signals from later incorporation of this multifunctional compound into the particle. This is similar to the case of the dicarbonyl hydroperoxide (DICARBROOH, Channel 2b) sharing two functionalities with the carbonyl hydroperoxide (CARBROOH), so it may contribute to the signal at m/z = 183. However, because the m/z = 183 and m/z = 185 ions are distinct and dominant components of the initial organic growth, and since their trends do not deviate from their respective +32 amu ion partners (m/z = 215, m/z = 217) with later incorporation of the suggested ions for the multifunctionals (m/z's 197, 199, 229, and 231), they are still likely representative ion fragments from the carbonyl hydroperoxide-derived PHA (KAHAP) and the hydroxy hydroperoxide-derived PHA (HAHAP).

Particle-Phase Peroxyhemiacetal Formation. The surface matrix of an aerosol particle probably enhances PHA generation by lowering energetic barriers or chemically catalyzing the reaction at the surface,[55] similar to dihydrofuran (DHF) formation.[38] Still, a lower energy barrier was not sufficient to see evidence of AHAP formed from the second-generation hydroperoxide (ROOH) in the AMS spectra. Its higher vapor pressure, further reaction with OH or photolysis, as well as the delay to aldehyde formation are all likely reasons why the fate of the ROOH is purely gas-phase oxidation. The nature of the particle interface and bulk are difficult to establish when considering such heterogeneous processes in the current study, but some insights into the chemistry behind PHA formation come from the study by Antonovskii and Terent'ev.[56] First, they find that aldehydes are more likely than ketones to participate in α-hydroxy peroxide formation because they exhibit greater polarity and polarizability in their

dx.doi.org/10.1021/jp211531h | J. Phys. Chem. A 2012, 116, 6211−6230

C═O containing π bond. Hence, PHA formation from the second-generation carbonyl is not considered for this discussion. Second, they observed that the forward reaction to α-hydroxy peroxide dominated over backward dissociation when run in polar solvents (chloroform, diisopropyl ether, or hexanol). Considering earlier discussion on the characteristic of the aerosol chemistry, PHA formation may be hindered if the aerosol matrix is not sufficiently polar, as there is a large mass fraction of organic described by CH family ions. Lastly, Antonovskii and Terent'ev observed stable α-hydroxy peroxides at 20 and 40 °C, but they note that α-hydroxy peroxides are less thermally stable than the hydroperoxide. This could mean the peroxides do not survive well through the thermal vaporization (600 °C) and ionization process in the techniques here. This may possibly explain the small mass concentrations for the characteristic PHA ions relative to the total organic mass. Still, in this study we keep in mind that the aldehyde formation relies on photolysis of a well-positioned α-carbonyl hydroperoxide. So, concentration, timing, and chemistry of the aerosol all have to be in harmony to facilitate PHA formation.

Cyclic Hemiacetal Formation. The 1,4-hydroxycarbonyl (OHCARB) has been theorized[38] and found experimentally to heterogeneously react, isomerizing to a cyclic hemiacetal (CHA) in the particle[9,11] or on chamber walls in an acid-catalyzed process.[15] These heterogeneous reactions have been found to happen within a time frame of approximately 1 h.[9,11,15] Conversion of the CHA to a DHF is sensitive to water vapor;[57] under low relative humidity environments, it will dehydrate to form a higher vapor pressure DHF compound that can partition back to the gas-phase and undergo further reaction with OH or O_3. A summary of these reactions is shown in Channel 3, Figure 1. Higher relative humidity conditions will slow the dehydration process, and OH reaction with the 1,4-hydroxycarbonyl (OHCARB) will more likely be its fate.[58] Under the current experimental conditions, DHF reaction with O_3 is expected to dominate after 2.5 h of irradiation when O_3 produced over time surpasses 5 ppb, the limit at which reaction with O_3 is competitive with reaction of the available OH radical ($\sim 2 \times 10^6$ molecules cm^{-3}). This is based on reaction rate coefficients available in the literature on 4,5-dihydro-2-methylfuran, using $k_{DHF-OH} = 2.18 \times 10^{-10}$ molecules cm^{-3} s^{-1} and $k_{DHF-O_3} = 3.49 \times 10^{-15}$ molecules cm^{-3} s^{-1}.[59] This provides an interesting problem to consider when thinking of the true lifecycle of the starting alkane and its ultimate generation of a higher vapor pressure unsaturated compound susceptible to oxidation and relevant for further SOA formation. Kinetic study of this heterogeneous conversion under OH radical initiated photoxidation of $C_{11}-C_{17}$ alkanes in the presence of NO_x suggests that the conversion to the CHA is fast in dry air, while the dehydration of the CHA to the DHF occurs on the order of ~15 min.[12]

CHA formation may be possible via the photolysis of the hydroperoxide (ROOH) in Channel 3 or through a fifth-generation multifunctional commpound analogously cyclizing (Channel 2aii), though the resulting CHA has an extra carbonyl group as seen in Figure 1. Sufficient evidence does not exist to confirm CHA formation for this study despite low relative humidity experimental conditions. If the CHA is formed as $C_{12}H_{24}O_2$, an AMS fragment at m/z = 183 ($C_{12}H_{23}O^+$) generated from loss of the −OH group[9] is possible. However, this fragment is more appropriately assigned as a characteristic ion of the carbonyl hydroperoxide (CARBROOH)-derived PHA instead as discussed earlier. In experiments carried out in the presence of NO_x, which are not reported here, the m/z = 183 ion is observed distinctly and does not pair with m/z = 215, making the current assignment consistent with the expected gas-phase mechanism under low-NO_x conditions. Since a distinct time trend indicating formation of the CHA in the particle-phase is not yet fully distinguished from the nominal mass at m/z = 183, the kinetics under the current experimental conditions cannot be modeled. On another note, the nature of the particle acidity is different than that of previous studies, as it is thought that adsorbed HNO_3 on the particle surface catalyzed the heterogeneous conversion to the DHF.[11,12] Under these low-NO_x conditions, HNO_3 formation is not considered. While the particle character shows enhancement of acidity as tracked by the AMS ion CO_2^+ at m/z = 44, there is still a large mass fraction described by the CH family ions, consistent with the many reduced fragments that could be derived from these long chain products. Considering that the simulated production of the 1,4-hydroxycarbonyl is only around 0.6 ppb in the gas-phase (without sinks) and the unclear nature of the particle acidity, if the cyclization and dehydration to the DHF does occur, the amount that formed was probably small, indiscernible in the AMS signal.

Heterogeneous Chemistry versus Gas-Phase Oxidation. We have currently considered two routes to formation of SOA through heterogeneous reactions. We see evidence of PHA formation derived from many semivolatile hydroperoxide species formed in all reaction channels, but we cannot confirm formation of the CHA from the 1,4-hydroxycarbonyl (OHCARB) at this time. Furthermore, the contributions to the SOA mass from pure gas-particle partitioning and heterogeneous chemistry of the hydroperoxide compounds to the SOA mass are unclear. To explore this, we roughly estimate the mass contributions of organic from five select semivolatiles that have been highlighted in a previous discussion: (1) carbonyl hydroperoxide (CARBROOH), (2) hydroxy hydroperoxide (OHROOH), (3) hydroxycarbonyl hydroperoxide (OHCARBROOH), (4) dicarbonyl hydroperoxide (DICARBROOH) and (5) 1,4-hydroxycarbonyl (OHCARB). Using the roughly estimated gas-phase concentrations of these species as monitored by the CIMS, the subcooled pure component liquid vapor pressure estimates (C_i^o), and the organic mass concentration from the AMS (as shown in Figure 2a), we assume that gas-particle equilibrium is established quickly so that the instantaneous contribution of each compound in the particle-phase is calculated by eq 1:

$$C_{pi} = \frac{C_{org} C_{gi}}{\gamma_i C_i^0} \quad (1)$$

where C_{pi} is the mass concentration of species i in the particle phase [$\mu g\ m^{-3}$], C_{org} is the mass concentration of organic aerosol in [$\mu g\ m^{-3}$], C_{gi} is the mass concentration of species i in the gas phase [$\mu g\ m^{-3}$], γ_i is the activity coefficient of species i in the bulk aerosol solution (assumed as 1 here), and C_i^0 = the subcooled pure component liquid vapor pressure of species i [$\mu g\ m^{-3}$].

The result of this analysis is presented in Figure 9. Note that we estimate the organic mass only up to 18 h because we utilized species monitored at $m/z \geq 300$, available only from the January experiment. We see that just under 10 $\mu g\ m^{-3}$ of organic is expected each from the dicarbonyl hydroperoxide (DICARBROOOH), carbonyl hydroperoxide (CARBROOH),

dx.doi.org/10.1021/jp211531h | J. Phys. Chem. A 2012, 116, 6211−6230

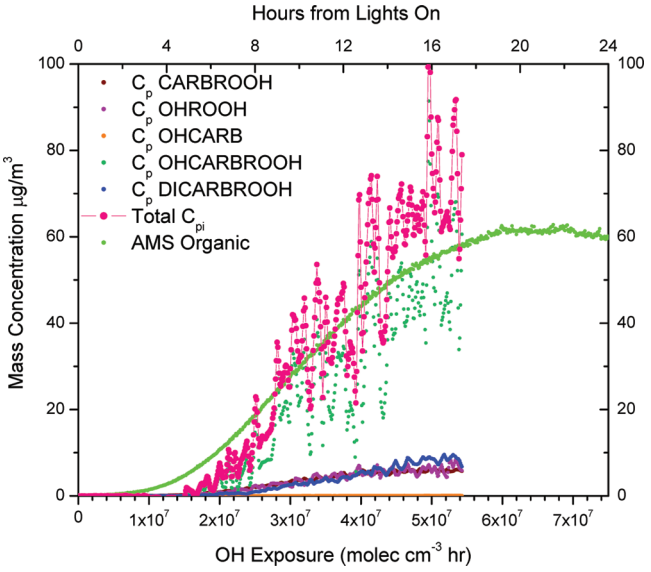

Figure 9. Rough estimate of total organic mass attributed to gas-to-particle phase partitioning from select semivolatiles (pink circles with line) as compared to the AMS organic trace (bright green). Individual contributions from each species are shown: (1) carbonyl hydroperoxide (CARBROOH, wine-colored circles), (2) hydroxy hydroperoxide (OHROOH, purple circles), (3) 1,4-hydroxycarbonyl (OHCARB, orange circles), (4) hydroxycarbonyl hydroperoxide (OHCARBROOH, teal circles), and (5) dicarbonyl hydroperoxide (DICARBROOH, blue circles).

and the hydroxy hydroperoxide (OHROOH). The 1,4-hydroxycarbonyl (OHCARB) makes negligible mass, and this is consistent with the small amount expected to form from the gas-phase chemistry and the absence of an AMS ion for the CHA. The hydroxycarbonyl hydroperoxide (OHCARBROOH) is expected to make up the majority of the organic mass ($\sim$ 60 μg m^{-3}). The total contributions of these species to organic mass is $C_{ptot} = \sum_i C_{pi}$. Thus, partitioning from just four semivolatile hydroperoxides could explain the majority of the organic growth observed after 5 h of irradiation. However, a small amount of organic was formed previously and is not fully described by equilibrium partitioning of these semivolatiles.

The uncertainty in the estimated gas-phase concentrations could resolve the appearance of organic growth prior to significant contributions from partitioning, but based on the well-paired m/z < 200 and m/z > 200 ions that differ by 32 amu, it is overwhelmingly likely that the fragments come from the same compound (their respective PHA). These ions also begin to appear prior to 5 h with aldehyde formation in the case of the carbonyl hydroperoxide (CARBROOH) and the hydroxy hydroperoxide (OHROOH) (see Figure 8a,b). So the early gap between the measurement and estimated organic mass may be due to PHA formation initiating aerosol growth. In light of the AMS measurements of characteristic PHA ions and the estimated mass from partitioning of the same hydroperoxide semivolatiles, it is difficult to tell whether these semivolatiles would be completely in the particle-phase as PHAs or in molecular form. In addition, later more functionalized compounds may partition in without conversion to PHA formation right away, as in the lag between gas-phase aldehyde formation and PHA ion appearance observed for the hydroxycarbonyl hydroperoxide (OHCARBROOH) and for that of the dicarbonyl hydroperoxide (DICARBROOH). However, since aldehyde formation is fairly coincident with most of the higher generation multifunctionals (OHCARBROOH, DICARBROOH) in the gas-phase, PHA formation as a mechanism for their incorporation into the particle phase cannot be ruled out. Full treatment of the kinetics of the heterogeneous chemistry require mass closure on the contribution of PHA mass to the organic present. While the AMS ions presented support PHA formation, their mass concentration signals do not account for the total mass of the derived PHA in the particle phase. Recall that the ions discussed do not include the side of the molecule that contains varying carbon lengths from the aldehyde that reacted with the hydroperoxide species. This provides a multitude of possible PHA structures. Second, being such a large molecule, PHA mass would certainly be distributed in the AMS spectrum among many possible fragmentation pathways. To truly understand these aspects, synthesis of these compounds would be required as an AMS standard to understand the full spectrum distribution.

■ ATMOSPHERIC IMPLICATIONS

Presented here is the first experimental study of SOA formation from the long-chain alkanes under low-NO_x conditions, such that RO_2 + HO_2 chemistry dominates the fate of the RO_2 radical. This regime of chemistry is typical of a region relatively isolated from NO_x sources and where trace VOC concentrations are too low to sustain RO_2 self-reaction. It is a challenge to simulate this chemistry in most laboratory chambers under atmospherically pristine conditions at which NO_x levels are typically tens to low hundreds of pptv. The gas-phase measurements of this study are consistent with chemistry expected for NO_x levels toward this range. Further, a regime of "slow" chemistry that lengthens the RO_2 lifetime sufficiently to allow for alkyl peroxy radical rearrangement through a 1,6-H shift is relevant to pristine conditions (ppt levels of NO_x, HO_2, and low [OH] $\sim 1.2 \times 10^5$ molecules cm^{-3}).[46] Achieving such conditions further challenges the design of environmental chamber studies. Although many challenges remain in simulating and spanning the range of "atmospherically relevant" conditions using environmental chambers, fundamental studies such as that described here address the fundamental chemistry in a regime relevant for closing the gap in the VOC and SOA budgets.

A myriad of compounds is formed in long-chain alkane photooxidation via functionalization and fragmentation pathways in the gas phase. For dodecane, 19 gas-phase species were monitored by the CIMS, and many compared well to a simulation with an abbreviated chemical mechanism based on the MCM 3.2. The gas-phase mechanism generally captures the observations only using four generations of explicit chemistry. Further work on empirical quantification and branching ratios of the gas-phase routes in the mechanism is needed, but was hindered for this study due to the lack of available standards and difficulties associated with experimental handling. Nonetheless, this study fundamentally captures the chemical framework representative of low initial organic loading of a longer-lived species (in terms of reaction with OH) while in the relative absence of NO_x that can be extended to alkanes of different lengths and structures. Current work is ongoing to understand the chemistry of SOA formation from other C_{12} alkanes of branched and cyclic conformations.

Mechanisms of particle formation emerge from comparison of the gas-phase mechanism and known heterogeneous chemistry. While there is evidence supporting the formation

dx.doi.org/10.1021/jp211531h | J. Phys. Chem. A 2012, 116, 6211−6230

of PHAs, confirmation of the heterogeneous conversion of the 1,4-hydroxycarbonyl to the CHA is lacking, but the amount that formed was probably small. A powerful approach to confirming direct partitioning of specific gas-phase compounds is through comparison of CIMS gas-phase time trends and corresponding characteristic ion fragments from the AMS. The paired (32 amu difference) high m/z > 100 AMS fragments identified were instrumental in deriving more molecular structure information in support of PHA formation. Comparisons of time trends provide insight into the chemistry of the partitioning, as seen, for example, with the decreasing delay between appearance of characteristic AMS ions and gas-phase product growth with increasing oxidation of the parent molecule. A rough estimate shows that much of the organic growth can be described by theoretical partitioning estimates of select semivolatile hydroperoxides. Still, better mass closure on the semivolatiles in the system in the gas and particle-phases could provide greater insight into the kinetic and equilibrium effects on SOA formation from dodecane.

The degree of generational development in the gas-phase photooxidation of this long-chain alkane over the extended chamber experiments is quite remarkable. While the majority of the gas-phase product distribution (almost two-thirds of the carbon) is developed within the first 20 h of photoxidation, SOA formation clearly involves the further oxidation of the third-generation carbonyl hydroperoxide, which peaks about 8 h earlier. This chemical development occurs much later than typical experimental time scales for chamber experiments, which highlights the need for simulating extended oxidation to truly capture the SOA formation process.

While the chemical composition of the gas and aerosol phases was well resolved with the techniques used in this study, challenges still exist in understanding the nature of the particle phase, as this can have profound effects on the further chemical aging of the particles.[60] This aging could be manifested in the formation of alkane-derived PHAs. In regards to time scale, the current work focuses on oxidative processes in the gas phase affecting the chemical development of the particle phase, although the possibility of photolysis or reactions with OH of the aerosol products may become more important under extended photoxidation time scales. A better understanding of these and other factors that potentially affect SOA chemical evolution might address issues such as the observed "glassy" nature of some SOA.[61,62] Extrapolating the present study to the atmosphere suggests that (1) hydroperoxide and PHA species are likely to be in the particle phase for alkane-derived aerosol under low-NO_x conditions, and (2) with the possibility of viscous phases that affect further chemical aging in the aerosol phase, the lifetimes of these products could be extended, lending themselves to long-range transport and a more complicated assessment of the SOA life cycle.

■ ASSOCIATED CONTENT

Supporting Information

The Supporting Information includes (1) A table with calculated lifetimes of RO_2 with RO_2, HO_2, NO, and NO_2 under varying NO_x conditions, (2) table of O:C and volatility, (3) figures on AMS and CIMS measurements across all experiments, (4) alternative positive mode ions for CIMS negative mode ions, and (5) simulations of varying NO concentration. This information is available free of charge via the Internet at http://pubs.acs.org.

■ AUTHOR INFORMATION

Corresponding Author

*E-mail: seinfeld@caltech.edu.

Notes

The authors declare no competing financial interest.

■ ACKNOWLEDGMENTS

This work was supported by the Office of Science (Biological and Environmental Research), U.S. Department of Energy Grant (DE-SC 0006626), and National Science Foundation Grants AGS-1057183 and ATM-0650061. We acknowledge John D. Crounse and Jason M. St. Clair for helpful discussions on CIMS data analysis, Reddy L. N. Yatavelli and ManNin Chan for useful discussions, and Andreas Zuend, Xuan Zhang, and Steve Compernolle for assistance with the vapor-pressure estimations. L.D.Y., J.S.C., and C.L.L. were supported by National Science Foundation Graduate Research Fellowships.

■ REFERENCES

(1) Ravishankara, A. R. *Chem. Rev.* **2003**, *103*, 4505−4508.
(2) Jimenez, J. L.; Canagaratna, M. R.; Donahue, N. M.; Prevot, A. S. H.; Zhang, Q.; Kroll, J. H.; DeCarlo, P. F.; Allan, J. D.; Coe, H.; Ng, N. L.; et al. *Science* **2009**, *326*, 1525−1529.
(3) Kroll, J. H.; Donahue, N. M.; Jimenez, J. L.; Kessler, S. H.; Canagaratna, M. R.; Wilson, K. R.; Altieri, K. E.; Mazzoleni, L. R.; Wozniak, A. S.; Bluhm, H.; et al. *Nat. Chem.* **2011**, *3*, 133−139.
(4) Robinson, A. L.; Donahue, N. M.; Shrivastava, M. K.; Weitkamp, E. A.; Sage, A. M.; Grieshop, A. P.; Lane, T. E.; Pierce, J. R.; Pandis, S. N. *Science* **2007**, *315*, 1259−1262.
(5) Schauer, J. J.; Kleeman, M. J.; Cass, G. R.; Simoneit, B. R. T. *Environ. Sci. Technol.* **1999**, *33*, 1578−1587.
(6) Schauer, J. J.; Kleeman, M. J.; Cass, G. R.; Simoneit, B. R. T. *Environ. Sci. Technol.* **2002**, *36*, 1169−1180.
(7) Presto, A. A.; Miracolo, M. A.; Kroll, J. H.; Worsnop, D. R.; Robinson, A. L.; Donahue, N. M. *Environ. Sci. Technol.* **2009**, *43*, 4744−4749.
(8) Presto, A. A.; Miracolo, M. A.; Donahue, N. M.; Robinson, A. L. *Environ. Sci. Technol.* **2010**, *44*, 2029−2034.
(9) Lim, Y. B.; Ziemann, P. J. *Environ. Sci. Technol.* **2005**, *39*, 9229−9236.
(10) Lim, Y. B.; Ziemann, P. J. *Environ. Sci. Technol.* **2009**, *43*, 2328−2334.
(11) Lim, Y. B.; Ziemann, P. J. *Aerosol Sci. Technol.* **2009**, *43*, 604−619.
(12) Lim, Y. B.; Ziemann, P. J. *Phys. Chem. Chem. Phys.* **2009**, *11*, 8029−8039.
(13) Talukdar, R. K.; Mellouki, A.; Gierczak, T.; Barone, S. *Int. J. Chem. Kinet.* **1994**, *26*, 973−990.
(14) Atkinson, R. *J. Phys. Chem. Ref. Data* **1997**, *26*, 215−290.
(15) Atkinson, R.; Arey, J.; Aschmann, S. M. *Atmos. Environ.* **2008**, *42*, 5859−5871.
(16) Tyndall, G. S.; Cox, R. A.; Granier, C.; Lesclaux, R.; Moortgat, G. K.; Pilling, M. J.; Ravishankara, A. R.; Wallington, T. J. *J. Geophys. Res.* **2001**, *106*, 12157−12182.
(17) Kroll, J. H.; Seinfeld, J. H. *Atmos. Environ.* **2008**, *42*, 3593.
(18) Lelieveld, J.; Butler, T. M.; Crowley, J. N.; Dillon, T. J.; Fischer, H.; Ganzeveld, L.; Harder, H.; Lawrence, M. G.; Martinez, M.; Taraborrelli, D.; et al. *Nature* **2008**, *452*, 737−740.
(19) Ren, X.; Olson, J. R.; Crawford, J. H.; Brune, W. H.; Mao, J.; Long, R. B.; Chen, Z.; Chen, G.; Avery, M. A.; Sachse, G. W.; et al. *J. Geophys. Res.* **2008**, *113*, D05310.
(20) Wolfe, G. M.; Thornton, J. A.; Bouvier-Brown, N. C.; Goldstein, A. H.; Park, J.-H.; McKay, M.; Matross, D. M.; Mao, J.; Brune, W. H.; LaFranchi, B. W.; et al. *Atmos. Chem. Phys.* **2011**, *11*, 1269−1294.
(21) Cocker, D. R.; Flagan, R. C.; Seinfeld, J. H. *Environ. Sci. Technol.* **2001**, *35*, 2594−2601.

(22) Keywood, M. D.; Varutbangkul, V.; Bahreini, R.; Flagan, R. C.; Seinfeld, J. H. *Environ. Sci. Technol.* **2004**, *38*, 4157−4164.
(23) St Clair, J. M.; McCabe, D. C.; Crounse, J. D.; Steiner, U.; Wennberg, P. O. *Rev. Sci. Instrum.* **2010**, *81*, 6.
(24) Paulot, F.; Crounse, J. D.; Kjaergaard, H. G.; Kroll, J. H.; Seinfeld, J. H.; Wennberg, P. O. *Atmos. Chem. Phys.* **2009**, *9*, 1479−1501.
(25) Crounse, J. D.; McKinney, K. A.; Kwan, A. J.; Wennberg, P. O. *Anal. Chem.* **2006**, *78*, 6726−6732.
(26) Huey, L. G.; Villalta, P. W.; Dunlea, E. J.; Hanson, D. R.; Howard, C. J. *J. Phys. Chem.* **1996**, *100*, 190−194.
(27) Crutzen, P.; Williams, J.; Pöschl, U.; Hoor, P.; Fischer, H.; Warneke, C.; Holzinger, R.; Hansel, A.; Lindinger, W.; Scheeren, B.; Lelieveld, J. *Atmos. Environ.* **2000**, *34*, 1161−1165.
(28) Jayne, J. T.; Leard, D. C.; Zhang, X.; Davidovits, P.; Smith, K. A.; Kolb, C. E.; Worsnop, D. R. *Aerosol Sci. Technol.* **2000**, *33*, 49−70.
(29) DeCarlo, P. F.; Kimmel, J. R.; Trimborn, A.; Northway, M. J.; Jayne, J. T.; Aiken, A. C.; Gonin, M.; Fuhrer, K.; Horvath, T.; Docherty, K. S.; et al. *Anal. Chem.* **2006**, *78*, 8281−8289.
(30) Canagaratna, M.; et al. *Mass Spectrom. Rev.* **2007**, *26*, 185−222.
(31) Loza, C. L.; Chhabra, P. S.; Yee, L. D.; Craven, J. S.; Flagan, R. C.; Seinfeld, J. H. *Atmos. Chem. Phys. Disc.* **2011**, *11*, 24969−25010.
(32) Jenkin, M. E.; Saunders, S. M.; Pilling, M. J. *Atmos. Environ.* **1997**, *31*, 81−104.
(33) Saunders, S. M.; Jenkin, M. E.; Derwent, R. G.; Pilling, M. J. *Atmos. Chem. Phys.* **2003**, *3*, 161−180.
(34) Kwok, E. S.; Atkinson, R. *Atmos. Environ.* **1995**, *29*, 1685−1695.
(35) Carter, W. P.; Cocker, D. R. I.; Fitz, D. R.; Malkina, I. L.; Bumiller, K.; Sauer, C. G.; Pisano, J. T.; Bufalino, C.; Song, C. *Atmos. Environ.* **2005**, *39*, 7768−7788.
(36) Wang, J.; Doussin, J. F.; Perrier, S.; Perraudin, E.; Katrib, Y.; Pangui, E.; Picquet-Varrault, B. *Atmos. Meas. Tech.* **2011**, *4*, 2465−2494.
(37) Sander, S. P.; Abbatt, J.; Barker, J. R.; Burkholder, J. B.; Friedl, R. R.; Golden, D. M.; Huie, R. E.; Kolb, C. E.; Kurylo, M.; Moortgat, G. K.; et al., Chemical kinetics and photochemical data for use in atmospheric studies, Evaluation No. 17. JPL Publication 10-6, 2011; http://jpldataeval.jpl.nasa.gov.
(38) Dibble, T. S. *Chem. Phys. Lett.* **2007**, *447*, 5−9.
(39) Vaghjiani, G.; Ravishankara, A. *J. Geophys. Res.* **1989**, *94* (D3), 3487−3492.
(40) Vaghjiani, G. L.; Ravishankara, A. R. *J. Chem. Phys.* **1990**, *92*, 996−1003.
(41) Baasandorj, M.; Papanastasiou, D. K.; Talukdar, R. K.; Hasson, A. S.; Burkholder, J. B. *Phys. Chem. Chem. Phys.* **2010**, *12*, 12101−12111.
(42) Atkinson, R. *J. Phys. Chem. Ref. Data, Monogr.* **1994**, *2*, 1−216.
(43) Atkinson, R.; Arey, J. *Chem. Rev.* **2003**, *103*, 4605−4638.
(44) Matsunaga, A.; Ziemann, P. J. *Aerosol Sci. Technol.* **2010**, *44*, 881−892.
(45) Loza, C. L.; Chan, A. W. H.; Galloway, M. M.; Keutsch, F. N.; Flagan, R. C.; Seinfeld, J. H. *Environ. Sci. Technol.* **2010**, *44*, 5074−5078.
(46) Crounse, J. D.; Paulot, F.; Kjaergaard, H. G.; Wennberg, P. O. *Phys. Chem. Chem. Phys.* **2011**, *13*, 13607−13613.
(47) Hasson, A. S.; Tyndall, G. S.; Orlando, J. J. *J. Phys. Chem. A* **2004**, *108*, 5979−5989.
(48) Spencer, K. M.; Beaver, M. R.; Clair, J. M. S.; Crounse, J. D.; Paulot, F.; Wennberg, P. O. *Atmos. Chem. Phys. Disc.* **2011**, *11*, 23619−23653.
(49) Compernolle, S.; Ceulemans, K.; Müller, J.-F. *Atmos. Chem. Phys.* **2011**, *11*, 9431−9450.
(50) Donahue, N. M.; Kroll, J. H.; Pandis, S. N.; Robinson, A. L. *Atmos. Chem. Phys. Disc.* **2011**, *11*, 24883−24931.
(51) Aiken, A. C.; DeCarlo, P. F.; Jimenez, J. L. *Anal. Chem.* **2007**, *79*, 8350−8358.
(52) Ziemann, P. J. *J. Phys. Chem. A* **2003**, *107*, 2048−2060.
(53) Matsunaga, A.; Docherty, K. S.; Lim, Y. B.; Ziemann, P. J. *Atmos. Environ.* **2009**, *43*, 1349−1357.
(54) Kern, W.; Spiteller, G. *Tetrahedron* **1996**, *52*, 4347−4362.
(55) Tobias, H. J.; Ziemann, P. J. *Environ. Sci. Technol.* **2000**, *34*, 2105−2115.
(56) Antonovskii, V. L.; Terent'ev, V. A. *J. Org. Chem. U.S.S.R. (Engl. Transl.)* **1967**, *3*, 972.
(57) Holt, T.; Atkinson, R.; Arey, J. *J. Photochem. Photobiol., A* **2005**, *176*, 231−237.
(58) Aschmann, S. M.; Arey, J.; Atkinson, R. *J. Atmos. Chem.* **2003**, *45*, 289−299.
(59) Martin, P.; Tuazon, E. C.; Aschmann, S. M.; Arey, J.; Atkinson, R. *J. Phys. Chem. A* **2002**, *106*, 11492.
(60) Ziemann, P. J. *Faraday Discuss.* **2005**, *130*, 469−490.
(61) Virtanen, A.; Joutsensaari, J.; Koop, T.; Kannosto, J.; Yli-Pirila, P.; Leskinen, J.; Makela, J. M.; Holopainen, J. K.; Poschl, U.; Kulmala, M.; et al. *Nature* **2010**, *467*, 824−827.
(62) Vaden, T. D.; Imre, D.; Beránek, J.; Shrivastava, M.; Zelenyuk, A. *Proc. Natl. Acad. Sci. U. S. A.* **2011**, *108*, 2190−2195.